NASA TECHNICAL NOTE

NASA TN D-8081

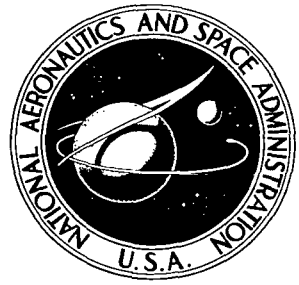

NASA TN D-8081

EFFECT OF SLOT WIDTH ON TRANSITION AND NOISE ATTENUATION OF A FLAT SOUND SHIELD IN A MACH 6 WIND TUNNEL

P. Calvin Stainback, William D. Harvey, and Andrew J. Srokowski

Langley Research Center
Hampton, Va. 23665

NATIONAL AERONAUTICS AND SPACE ADMINISTRATION • WASHINGTON, D. C. • NOVEMBER 1975

1. Report No. NASA TN D-8081	2. Government Accession No.	3. Recipient's Catalog No.
4. Title and Subtitle EFFECT OF SLOT WIDTH ON TRANSITION AND NOISE ATTENUATION OF A FLAT SOUND SHIELD IN A MACH 6 WIND TUNNEL		5. Report Date November 1975 6. Performing Organization Code
7. Author(s) P. Calvin Stainback, William D. Harvey, and Andrew J. Srokowski		8. Performing Organization Report No. L-10403 10. Work Unit No. 505-06-41-01
9. Performing Organization Name and Address NASA Langley Research Center Hampton, Va. 23665		11. Contract or Grant No.
12. Sponsoring Agency Name and Address National Aeronautics and Space Administration Washington, D.C. 20546		13. Type of Report and Period Covered Technical Note 14. Sponsoring Agency Code
15. Supplementary Notes		

16. Abstract

A technique for attenuating the noise radiated into the test section from the turbulent boundary layer on the walls of wind tunnels is the use of sound radiation shields. An experimental and theoretical study of a sound shield concept was conducted. This conceptual sound shield model is planar with a sharp flat-plate leading edge faired into an array of rods alined nearly parallel to the local flow.

For a ratio of gap diameter to rod diameter of 0.16, the flow was laminar over the entire model at a maximum local length Reynolds number of 14×10^6. A 45-percent reduction of the tunnel free-stream root-mean-square pressure level was measured within the shielded region for this gap width when the boundary layers on the rods were laminar. For smaller ratios of gap diameter to rod diameter of 0.12 and 0.068, a 40-percent pressure reduction was obtained with laminar flow on the model. The smaller ratios of gap diameter to rod diameter resulted in substantial reductions in the transition Reynolds number.

17. Key Words (Suggested by Author(s)) Supersonic wind tunnels Sound attenuation Boundary-layer laminarization Research and support facilities (Air)	18. Distribution Statement Unclassified – Unlimited Subject Category 09		
19. Security Classif. (of this report) Unclassified	20. Security Classif. (of this page) Unclassified	21. No. of Pages 51	22. Price* $4.25

*For sale by the National Technical Information Service, Springfield, Virginia 22161

EFFECT OF SLOT WIDTH ON TRANSITION AND NOISE ATTENUATION OF A FLAT SOUND SHIELD IN A MACH 6 WIND TUNNEL

P. Calvin Stainback, William D. Harvey,
and Andrew J. Srokowski
Langley Research Center

SUMMARY

A technique for attenuating the radiated noise in supersonic and hypersonic wind tunnels by the use of a sound radiation shield in the test section has been investigated. The conceptual model was planar with a sharp flat leading edge faired into an array of 0.635-cm-diameter (0.25-in.) rods alined parallel to the local flow, with adjustable gaps between them for boundary-layer removal and laminarization by suction. Tests were conducted at Mach 6 for three gap widths over a wide range of unit Reynolds number for angles of attack of 5° and 10°.

For a ratio of gap diameter to rod diameter of 0.16, the flow was laminar at the most windward ray over the entire model length of 0.61 m (2 ft) at a maximum local length Reynolds number of 14×10^6. A 45-percent reduction of the tunnel free-stream normalized root-mean-square pressure level was measured within the shielded region for this gap spacing when the boundary layers on the rods were laminar. For the smaller ratios of gap diameter to rod diameter of 0.12 and 0.068, the transition Reynolds number and the sound attenuation decreased.

Boundary-layer calculations show that viscous blockage effects in the gaps are significant at low unit Reynolds numbers and smaller gap widths. The "flow quality" or uniformity of the mean flow field above the rods is satisfactory to within 1 rod diameter of the rod array. To prevent transmission of lee side noise back into the shielded region, theoretical and experimental results indicate that the cross flow in the gaps should be sonic.

Rod diameter, gap width, unit Reynolds number, and probably the leading-edge fairing determine the design and performance of a complete sound shield for wind tunnels. Present results suggest that the minimum ratio of gap diameter to rod diameter needed for laminar flow control and noise attenuation is 0.16. Large vacuum capacities may then be required for wind-tunnel sound shields of sufficient length and diameter to achieve test Reynolds numbers approaching 50×10^6.

INTRODUCTION

Unsteady disturbances in the test section of wind tunnels can have adverse effects on many aerodynamic characteristics. (See refs. 1 and 2.) These effects have been known for many years, and extensive efforts have been made to build low-turbulence subsonic wind tunnels. At high supersonic and hypersonic speeds, the major disturbance in the test section is the noise radiated from the turbulent boundary layer on the walls of the nozzle. (See refs. 2 and 3.) At the present time, these disturbances can only be eliminated by operating the wind tunnel at sufficiently low Reynolds numbers to maintain laminar boundary layers on the nozzle walls. Under these test conditions the boundary layers on models are also usually laminar and not representative of flight conditions. Therefore, the utility of wind tunnels under such conditions is limited.

The noise radiated from a turbulent boundary layer at supersonic speeds is very directional (ref. 4) and cylindrical shrouds have been used in attempts to prevent this noise from entering the test region (ref. 5). However, the boundary layer on the walls of the shroud usually becomes turbulent at relatively low Reynolds numbers, and this turbulent boundary layer radiates noise into the shielded region (ref. 5). The range of Reynolds number for which quiet operation is possible is then limited. In addition, some of the radiated noise impinging on the inner wall of the shroud would be reflected into the shielded region.

To be effective, a shroud or shield must isolate the test section from noise radiated by the turbulent boundary layer on the nozzle wall. Transition must also be delayed on the walls of the shield to sufficiently high Reynolds numbers to permit natural transition of the boundary layer on models. Furthermore, the shield must not produce any extraneous disturbances that can affect the mean flow in the test section or over models. Finally, the shield must be practical from an engineering and economic standpoint.

Except for complete isolation of a test region from radiated sound, the conceptual model described in reference 6 appeared to satisfy these requirements. This model consisted of an array of circular rods forming a planar surface. The rods were alined nearly parallel to the local flow with gaps between the rods for partial removal of the boundary layers on the rods. The rods then functioned somewhat like yawed infinite cylinders with a sweep angle approaching 90°. If the yawed infinite cylinder assumption is used, the transition Reynolds number would presumably depend on the diameter of the rods and not their length. Therefore, if rods with a small diameter are used, the transition Reynolds number based on length can be made sufficiently large. However, the diameter of the rods cannot be made arbitrarily small because of stiffness requirements.

The maximum transition length Reynolds number obtained on the stagnation line of the 0.61-m long (2-ft) conceptual rod model (ref. 6) was about 14×10^6 – almost an order

of magnitude larger than that measured on a flat plate in the same facility. The normalized root-mean-square pressure level in the free stream was reduced by about 45 percent in the partially shielded region of this model. The diameter of the rods and the gaps between them were 0.635 and 0.102 cm (0.25 and 0.040 in.), respectively, for the model of reference 6. When these dimensions were used to define requirements of a complete sound shield for a large tunnel, such as described in reference 1, the suction mass flow through the gaps was so large that the vacuum system for the shield became large and expensive. In order to reduce this suction mass flow and thereby reduce the size and cost of the vacuum system, tests have been conducted with the conceptual model (ref. 6) to determine the effect of reduced gap width on the maximum transition Reynolds numbers and noise attenuation. The purpose of this report is to present experimental results and detailed theoretical analysis of boundary-layer behavior and transition parameters showing the effects of reducing the gap width. Comparisons with results from reference 6 are also given. Some experimental results from this investigation are presented in reference 7.

SYMBOLS

Values are given in both the International System of Units (SI) and U.S. Customary Units. The measurements and calculations were made in U.S. Customary Units.

d	rod diameter, 0.635 cm (0.25 in.)
f	frequency
g	minimum physical width of gaps between rods
H	total enthalpy
M	Mach number
N_{St}	Stanton number
p	pressure
q	total velocity vector
R	unit Reynolds number, $\rho q/\mu$

R_d Reynolds number based on rod diameter, $(\rho q/\mu)_\infty d$

R_x Reynolds number based on distance from leading edge of model, $(\rho q/\mu)_\infty x$

R_θ Reynolds number based on boundary-layer momentum thickness, $(\rho w/\mu)_\infty \theta_w$

s surface distance around rods from windward stagnation line (measured in chordwise direction)

T absolute temperature

u chordwise velocity on rods in s-direction

w spanwise velocity on rods in x-direction

x distance along model from leading edge

y distance normal to top of rod model; also distance normal to rod surface

z transverse distance across top of rod model

α model angle of attack in tunnel free stream

α_{eff} local effective angle of attack of rods

δ boundary-layer thickness at $q/q_e = 0.995$

δ^* displacement thickness of boundary layer based on chordwise component of velocity, $\int_0^\delta \left[1 - \frac{\rho u}{(\rho u)_e}\right] dy$

θ_w spanwise momentum thickness, $\int_0^\delta \frac{\rho}{\rho_e}\left[\frac{w}{w_e} - \left(\frac{w}{w_e}\right)^2\right] dy$

μ viscosity coefficient

ρ mass density

ϕ chordwise angle measured around rods from windward stagnation line

Subscripts:

av	average
e	edge of rod boundary layers
g	at minimum physical width of gaps between rods ($\phi = 90^{o}$)
r	at $\phi = 180^{o}$ on leeward side of rods
$s\ell$	stagnation line of rods ($\phi = 0^{o}$)
T	transition
t	stagnation conditions downstream of normal shock
u	in chordwise direction
w	in spanwise direction
o	tunnel stagnation conditions
∞	local free-stream conditions behind oblique shock
$\overline{\infty}$	free stream in nozzle flow

Superscripts:

$\tilde{(\ )}$	root mean square of fluctuating quantity
$\bar{(\ )}$	steady-state value

APPARATUS AND TEST CONDITIONS

Model

The conceptual model of a sound shield used in the present tests is the same model used for the investigation reported in reference 6. Sketches and photographs of the model are shown in figure 1. Circular rods were used during this investigation, and the gaps between the rods were reduced from 0.102 cm (0.04 in.) used in reference 6 to 0.076 and 0.043 cm (0.030 and 0.017 in.).

The model consisted of a sharp flat plate that formed its leading edge, interchangeable circular rods alined nearly parallel to the local flow, and a support structure. The longitudinal rods were separated by spacers at the front and rear that provided the desired gap width between the rods. . The rear support member was a 1.27-cm-diameter (0.50-in.) rod. Two 0.159-cm-diameter (0.0625-in.) threaded rods were also used to support and maintain the correct gap width for the longitudinal rods (fig. 1(a)). These threaded rods passed through rectangular webs that were attached to the lee side of the rods to stiffen the rods. Small nuts screwed on the threaded rods on each side of the webs (fig. 1(a)) were used to maintain and adjust the correct gap width between the front and rear supports. The upper sketch in figure 1(a) shows a top view of the flat-plate leading edge and rod junction. The rods have a flat- to round-shaped transition section downstream of their junction with the flat-plate leading edge. The forward lower surface of the model (crosshatched area in fig. 1(a)) is a solid plate which shields the low-pressure side of the rods from noise generated by the boundary layer on the lower wall of the tunnel (fig. 1(b)). This lower plate also helps maintain base pressure inside the model when it is placed at an angle of attack as illustrated in figure 1(b). Sufficient pressure drop across the rod array to obtain sonic cross flow through the gaps was obtained by testing the model at an angle of attack. The purpose of sonic cross flow at the gaps is to prevent transmission of noise from the lee side of the model into the shielded region.

Two hollow rods (0.071-cm-thick (0.028-in.) walls) were instrumented with 21 thermocouples spaced evenly along their length and located at the top windward stagnation line. The diameter of the chromel-alumel thermocouple wires was 0.0127 cm (0.005 in.), and they were spotwelded to the inside surface of the hollow rods to form the thermocouple junctions. The leads were brought out at the rear of the model. The standard transient technique was used to measure the heating rates.

Five rods had pressure orifices located as illustrated in table I:

TABLE I.- LOCATION OF PRESSURE ORIFICES

Rod number (see fig. 1(a))	x		ϕ, deg
	cm	in.	
2	31.75	12.5	0
2	31.75	12.5	180
2	49.53	19.5	0
2	49.53	19.5	180
4	13.97	5.5	0
4	13.97	5.5	180
4	31.75	12.5	0
4	31.75	12.5	180
6	31.75	12.5	90
6	31.75	12.5	90
7	49.53	19.5	90
7	49.53	19.5	90
8	31.75	12.5	0
8	31.75	12.5	180
8	49.53	19.5	0
8	49.53	19.5	180

The pressure orifices were 0.102 cm (0.040 in.) in diameter. The length of the pressure tubing was minimized to reduce lag. Capacitance-type pressure transducers were used that had seven ranges. Either automatic or manual range change was available. The accuracy of all pressure transducers was 0.25 percent of the full-scale reading on the ranges used during these tests. Pressure data were continuously monitored during each test, and data were recorded only when the readings became constant with time.

Fluctuating Pitot Pressure Probe

The fluctuating pressures in the flow field of the rod model and in the free stream of the wind tunnel were measured by use of a pitot probe. The probe, pressure transducers, and data-reduction methods were similar to those described in reference 2 except that the design of the probe was changed. A drawing of the new probe is presented in figure 2. The new design incorporated two 0.317-cm-diameter (0.125-in.) pressure transducers into one probe rather than in two separate probes as used in reference 2. Two transducers are required in order to correct the data for the effects of vibration. The exposed transducer was mounted so that the pressure-sensing surface was flush with the end of the pitot probe. This transducer was exposed to the disturbances in the flow field as well as to any forces due to acceleration caused by vibration. The other transducer was recessed into the body of the probe and was therefore subjected only to the forces due to acceleration. The output of each transducer due to acceleration was matched from tests where the transducers were interchanged. The sensitivity of the power supply was then adjusted so that the outputs of each transducer due to a given acceleration level were equal. After the matching process, the transducers were calibrated. The net root-mean-square (rms) pressure was obtained by subtracting the mean square of the pressure indicated by the covered transducer from the mean square of the pressure measured by the exposed transducer and taking the square root of this difference. By using this technique, the effect of acceleration is removed from the net results.

During the present tests the pitot probe was at one location ($x = 38.6$ cm (15.2 in.), $y = 2.858$ cm (1.125 in.)) for all tests as illustrated in figure 3 which also shows the approximate location of the model in the wind tunnel and a schematic representation of the radiated sound field.

Wind Tunnel and Test Conditions

The model was tested in the Langley Mach 6 20-inch tunnel (ref. 8). Tests were conducted over a local unit Reynolds number range from 3.3×10^6 to 42.6×10^6 per m (1.0×10^6 to 13.0×10^6 per ft). The ratio of wall temperature to free-stream total temperature was about 0.62. Tests were conducted at angles of attack of 5° and 10°.

RESULTS

Boundary-Layer Calculations

The swept infinite cylinder theory described in reference 9 and applied in references 6 and 10 was used to calculate the boundary layer on the rods. The variations of boundary-layer thickness δ and boundary-layer displacement thickness δ^* at the physical minimum ($\phi = 90^o$) of the gaps with local unit Reynolds number are presented in figure 4. These results are from a "first-order" calculation wherein the pressure distribution around the rods (calculated by the method of refs. 6 and 10) was not modified to account for boundary-layer displacement effects. The figure shows that the boundary-layer displacement thickness at $\phi = 90^o$ can become large with respect to the gap size at low unit Reynolds numbers and small gap widths. Hence, the inviscid flow through the gaps will be significantly modified by viscous effects for these conditions.

Figure 4 also shows that the calculated boundary-layer thickness at the minimum of the gap δ_g ($\phi = 90^o$) becomes larger than the gap size for $R_\infty \approx 16.4 \times 10^6$, 6.6×10^6, and 4.3×10^6 per m (5×10^6, 2×10^6, and 1.3×10^6 per ft) for $g/d = 0.068$, 0.120, and 0.160, respectively. Therefore, when unit Reynolds numbers are reduced below these values, the flow in the gaps will be completely viscous and the present analysis based on the boundary-layer assumption is not valid. Of course, the validity of the first-order boundary-layer analysis will become questionable at somewhat higher unit Reynolds numbers than these values primarily because of δ^* displacement effects on the inviscid flow.

Velocity and Mach number profiles at the physical minimum area from the first-order calculation for the three gap widths considered are shown in figure 5 for R of 19.7×10^6 per m (6×10^6 per ft). The u/u_e velocity profiles have a distinct overshoot because of the large viscous heating by dissipation of the supersonic w component of velocity and the resulting reductions in density. (See ref. 11.) However, the Mach number profiles do not have an overshoot and as the ratio of gap width to rod diameter is reduced from $g/d = 0.16$ to 0.068, the extent of sonic flow is reduced from approximately 50 percent of the gap width to essentially zero. Thus, in order to obtain effective shielding of lee side noise for the smaller gap sizes and lower Reynolds numbers, expansion to sonic velocity will have to occur downstream of the geometric minimum; this requirement is discussed later in greater detail.

Pressure Measurements and Analysis

Rod static pressure.- Static pressures were measured at axial stations of x = 13.97, 31.75, and 49.53 cm (5.5, 12.5, and 19.5 in., respectively) on the rods of the model. Pres-

sures were measured on the windward ray ($\phi = 0^o$), at the physical minimum in the gap ($\phi = 90^o$), and on the lee side of the rods ($\phi = 180^o$). (See table I.) As mentioned previously, the establishment of sonic cross flow in the gaps is a major requirement for the proper operation of the shield. To help determine whether sonic cross flow was obtained, the pressures at $\phi = 180^o$ and $\phi = 90^o$ were expressed as ratios to those measured on the windward ray ($\phi = 0^o$). These pressure ratios are shown in figures 6(a) and 6(b).

All the pressure ratios on the lee side of the model (fig. 6(a)) are below 0.528 and indicate that sonic cross flow was obtained, at least in the inviscid flow, for all gap widths and at angles of attack of 5^o and 10^o. The pressure ratios at $\phi = 90^o$ (fig. 6(b)) for $g/d = 0.160$ are less than or equal to 0.528 for an angle of attack of 10^o and indicate that sonic cross flow was obtained in the inviscid flow at the geometric minimum. The trend with decreasing gap size and decreasing Reynolds number, particularly at an angle of attack of 5^o, is to increase the gap pressure ratio above 0.528. Thus, for these conditions the boundary-layer displacement effect evidently moves the minimum flow area toward the lee side of the rods, expansion to sonic pressure occurring at an aerodynamic minimum downstream of $\phi = 90^o$.

Simple inviscid, one-dimensional flow requires that $p_g/p_{sl} \leqq 0.528$ for sonic or critical cross flow in the gaps. However, the boundary layer on the rods will not permit uniform sonic flow at the minimum area of the gap and some of the boundary-layer flow will be subsonic. (See fig. 5.) Thus, when the boundary-layer thickness approaches one-half the gap size, the region of sonic flow is more limited. However, if p_r is appreciably less than $(0.528)p_{sl}$, the cross flow can expand to higher Mach numbers downstream of $\phi = 90^o$. If enough of the boundary-layer flow expands to sonic velocity downstream of the gaps, the propagation of sound from the lee side of the model back through the gaps into the shielded region would be more effectively blocked.

To illustrate this effect of flow expansion downstream of the gaps, the viscous gap flow illustrated in figure 5 for $g/d = 0.12$, for example, was expanded to $p_e/p_{sl} = 0.29$, which is close to the minimum pressure measured on the lee side of the model (fig. 6(a)). The computed profiles shown in figure 7 resulted. Comparison of these theoretical results with the corresponding profiles in figure 5 where sonic flow occurs over about 45 percent of the gap at $\phi = 90^o$ shows that this percentage can be increased to 78 percent at $\phi = 100^o$ provided the lee side pressure is sufficiently low. Hence, it may be anticipated that for the smaller Reynolds numbers and gap widths, the back side or plenum pressure of the sound shield may have to be reduced below 0.528 of the stream static pressure to reduce the transmission of lee side noise into the shielded test region.

The requirement that the pressure on the lee side of the sound shield be maintained at, or even below 0.528 of, the stream static pressure will also require expensive, large-

capacity, low-loss vacuum ducting for a wind-tunnel sound shield. However, recovery of the kinetic energy of the gap flow would be expected to reduce the ducting requirements. In order to ascertain how much kinetic energy of the gap flow could be recovered for an assumed ideal process, the calculated boundary-layer profiles at the gap ($\phi = 90^{\circ}$) for $g/d = 0.16$ were integrated to yield the average normal-shock pressure recovery in the gap. The normal-shock pressure recovery was obtained for each point on the resultant Mach number profile $\left(M_g = \sqrt{M_u^2 + M_w^2}\right)$ by assuming constant static pressure $\left(p_g = 0.528 p_{sl}\right)$ across the gap and applying Rayleigh's pitot formula. These recovery pressures were then integrated across the entire gap to give an average value. The average of the resultant Mach number was computed in the same way from the formula

$$M_{g,av} = \frac{2}{g}\int_0^{g/2} M_g \, dy$$

These average values are plotted in figure 8 against unit Reynolds number. The average resultant Mach number and normal-shock pressure recovery ratios drop from 4.1 and 13.9 (at $R_\infty = 32.8 \times 10^6$ per m (10×10^6 per ft)) to 3.5 and 9.8 (at $R_\infty = 9.84 \times 10^6$ per m (3×10^6 per ft)), respectively. The increasing boundary-layer thickness with decreasing Reynolds number has a substantial effect on the available pressure recovery. The values of available pressure recovery are based on normal-shock recovery which is probably optimistic because viscous dissipation and mixing downstream of the gap will reduce these normal-shock values further. However, the high levels of the normal-shock recovery pressures calculated and shown in figure 8 indicate that careful design of the vacuum manifold for a wind-tunnel sound shield may substantially increase the pressure recovery and thereby reduce the size and cost of the vacuum ducting system and increase the wind-tunnel run time.

Mean pitot pressures in model flow field.- A survey of the flow field of the model with $g/d = 0.12$ and $\alpha = 10^{\circ}$ was made with a multitube pitot rake located at $x = 38.6$ cm (15.2 in.). The results obtained in a horizontal plane 2.86 cm (1.125 in.) above the rods are presented in figure 9(a). Figure 9(b) presents the tunnel pitot pressure and corresponding Mach number calibration, 2.54 cm (1 in.) above the tunnel center line. The decrease in the levels of the pressure ratios in the model flow field (figs. 9(a) and 9(b)) with increasing Reynolds number is consistent with the decrease in tunnel free-stream pitot pressure and the corresponding Mach number increase with increasing Reynolds number. The slight downward slope of the data with increasing z in figure 9(a) is believed to be due to nonuniformities in the tunnel mean flow (ref. 12). The wavy spanwise irregularities observed for $R_\infty \geq 16.01 \times 10^6$ per m (4.88×10^6 per ft) may be due to the increased suction obtained at higher Reynolds numbers (decreased δ^*), although a definite correlation with gap location is not evident.

A survey of the pitot pressures was also made normal to the planar surface of the model above a rod located on the model center line. The results are shown in figure 9(c). Measured pitot pressures increased slightly as the distance from the windward ray increased from 0.635 to 3.175 cm (0.25 to 1.25 in.). Except at $R_\infty = 11.1 \times 10^6$ per m (3.4×10^6 per ft), the pitot pressures decreased significantly as the distance from the probe to the rod decreased below 1 rod diameter. The anomalous behavior at $R_\infty = 11.1 \times 10^6$ per m (3.4×10^6 per ft) may be due to the occurrence of transition or an indication of a change in the vortical flow structure on the rods as discussed previously (ref. 6). These vortices are believed to originate in the flow field of the model at the transition region between the flat plate and the circular rods. Although the flow uniformity appears to be good, some improvements may be possible by modification of the transition region.

Heat Transfer

The data obtained from the thermocouples on the windward ray were reduced to heating rates by using the calorimetric method with the effect of the curvature and thickness of the rod wall included in the calculation. These results are presented in the form of Stanton number as a function of local Reynolds number in figures 10(a), 10(b), and 10(c) for $g/d = 0.16$, 0.12, and 0.068, respectively. The heat-transfer results presented in reference 6 and repeated here in figure 10(a) show that the heating rates on the windward ray of the rods were similar to those for an isolated swept cylinder. That is, at a given unit Reynolds number, the Stanton number is constant with length Reynolds number when the boundary layer is either laminar or turbulent. The Stanton number increased only when transition occurred on the windward ray. The present results indicate that these trends for the Stanton number also apply to the present data with normalized gap widths of 0.12 and 0.068 (figs. 10(b) and 10(c)). The most important result shown in figure 10 is the marked decrease in the transition Reynolds numbers as the gap width is reduced. The transition Reynolds numbers are taken as those values where the heating rates first begin to increase above the laminar level. These transition data are discussed in the following section.

The level of laminar heating at the stagnation line agreed very well with the "uncorrected" first-order theory (with external pressure distributions determined by assuming $\delta^* = 0$) for $g/d = 0.16$ and 0.12. This result is shown more clearly in figure 11 where the Stanton numbers obtained by fairing horizontal lines through the laminar data of figure 10 are plotted against unit Reynolds number. However, when $g/d = 0.068$, the heating rates are much higher than the theoretical predictions. The reason for this result is not known at the present time since it was expected that the heating rates for this case would be lower than predictions due to viscous effects which would reduce the flow through the gaps and thereby reduce the cross-flow velocity gradient at the stagnation line. The

observed increase in the heating rate for $g/d = 0.068$ might be due to vortices generated by the flat-plate—rod fairing section as discussed in reference 6. If viscous effects restrict the flow through the gaps, the vortices could not readily pass through the gaps and would tend to modify the flow in the vicinity of the stagnation line. This possibility is supported somewhat by the data for $g/d = 0.068$ shown in figure 11. At the higher unit Reynolds numbers where the flow through the gaps is not as restricted as at lower unit Reynolds numbers, the heat transfer to the stagnation line appears to be approaching the laminar theory.

It was expected that theoretical solutions utilizing the calculated chordwise pressure distribution around the rods corrected for boundary-layer displacement effects would be in closer agreement with the data. Such solutions were obtained for $g/d = 0.12$ and the results are shown in figure 11. The heating rates for the corrected solutions are lower than the data, the difference increasing with decreasing Reynolds number. The reason for this increasing difference between the uncorrected and corrected theory is evident from the corresponding chordwise velocity distributions (computed by the one-dimensional cross-flow method of refs. 6 and 10) around the rods. These normalized chordwise velocity distributions are plotted against arc length in figure 12(a) for $g/d = 0.12$ and $R = 9.84 \times 10^6$ per m (3×10^6 per ft). The stagnation region velocity gradient is smaller when the δ^* correction is included. As the gap is approached, the corrected gradient becomes larger than that for the uncorrected curve. The magnitude of the velocity with δ^* corrections is lower and has a slight downstream shift of the sonic point because of the δ^* displacement effect. This effect also reduces the values of α_{eff} (see fig. 1) which are shown in figure 12(a) for this case. The corresponding stagnation-line velocity gradients are plotted in figure 12(b) against Reynolds number based on rod diameter. Since the δ^* correction tends to reduce the theory below the data for the $g/d = 0.12$ case (fig. 11), it may be concluded that the higher heating levels of the experimental data, for both $g/d = 0.068$ and 0.12, are probably due to the vortices mentioned previously. The decrease in slope of the corrected theoretical solutions (see dashed line in fig. 11) as the Reynolds number decreases is similar to the trend exhibited by the data for $g/d = 0.068$ when $R < 11.48 \times 10^6$ per m (3.5×10^6 per ft).

Transition

Transition Reynolds numbers were obtained from the heat-transfer data by estimating the highest Reynolds number where the Stanton number was consistent with laminar values. This was done by fairing a curve through the laminar and transitional Stanton numbers and taking the intersection of these two lines as the beginning of transition. Transition Reynolds numbers are presented in figure 11 as a function of the local unit Reynolds number for $g/d = 0.068$, 0.12, and 0.16. Transition data were also obtained by using the fluctuating pitot probe, and these data are discussed later. Figure 13 shows that

the largest transition length Reynolds numbers were approximately 14×10^6, 7×10^6, and 3×10^6 for $g/d = 0.16$, 0.12, and 0.068, respectively. Thus, there was a substantial reduction in the maximum transition Reynolds number as gap size was reduced. This reduction in transition Reynolds number is probably due to the fact that at a given unit Reynolds number the flow in the gaps becomes more viscous as the gap size is reduced. This condition restricts the flow through the gaps and the flow over the model becomes similar to the flow over a flat plate rather than to that of an isolated swept cylinder. This reasoning is supported by the transition data in figure 13 for $g/d = 0.068$. After transition moved onto the model, the variation of the transition Reynolds number with unit Reynolds number has about the same slope as that for a flat plate.

The transition data obtained from the heat-transfer results are presented in figure 14 in the form of distance from the leading edge to the location of transition as a function of unit Reynolds number. This figure better illustrates the similarity between the movement of transition on the flat plate and the rod model for $g/d = 0.068$ and 0.12 at angles of attack of 5° and 10°. However, for $g/d = 0.12$ and 0.16 and $\alpha = 10^\circ$, transition moves forward with increasing R_∞ more rapidly on the rod model than on a flat plate. These results again suggest that transition might be controlled by a different mechanism for the larger gap widths of $g/d = 0.16$ and 0.12 at $\alpha = 10^\circ$ than for the smaller gap widths and angles of attack.

The values of the unit Reynolds number where transition first moves onto the rod model at $\alpha = 10^\circ$ are plotted against g/d in figure 15. This figure illustrates the large effect of gap size on the transition Reynolds number and shows that the data for the rod model with $g/d = 0.068$ approach the value for the flat plate. (The flat-plate datum point was obtained by extrapolating the data from reference 12 to $x = 0.61$ m (24 in.).) For comparison with transition correlations on swept cylinders, the Reynolds number based on diameter of the rods is shown on the right-hand side of figure 15. The maximum transition Reynolds number based on rod diameter for $g/d = 0.16$ approaches the transition Reynolds numbers obtained on isolated swept cylinders with root disturbances (ref. 13). Therefore, if root (leading-edge) disturbances are dominant in the transition process on the present model, this ratio of gap width to rod diameter of $g/d = 0.16$ may provide the maximum transition Reynolds number attainable unless modification of the leading edge of the model can reduce the disturbances originating at the region of the flat plate and rod junction. However, the local inviscid flow and velocity gradients around the rods are much different from those on isolated cylinders because of the artifically induced cross flow produced by the angle of attack of the model and the mutual interference between adjacent rods. Because of these effects, a further increase in gap size may increase $R_{d,T}$ above the correlation level of about 2×10^5 (fig. 15).

Transition criteria other than R_d must also be considered to evaluate and extrapolate the performance of the present model to the design of a wind-tunnel sound shield.

According to Pfenninger (ref. 14), the stagnation-line momentum thickness Reynolds number is a valid transition criterion for swept cylinder flows. Figure 16(a) presents the calculated stagnation-line momentum thickness Reynolds number for laminar boundary layers, based on the streamwise boundary-layer profiles, as a function of unit Reynolds number. As expected, $R_{\theta,w,sl}$ varies as the square root of R_∞ when no δ^* correction is included. As gap size increases, the stagnation-line velocity gradient increases with a corresponding decrease in the level of the momentum thickness Reynolds number. Also shown in the figure for $g/d = 0.12$ is the variation of $R_{\theta,w,sl}$ with R_∞ when the δ^* correction for the velocity distribution (see fig. 12) is included in the theory. The increased level and change in slope as the Reynolds number decreases is consistent with a smaller stagnation-line velocity gradient with increasing δ^*. Also shown in figure 16(a) are the values of $R_{\theta,w,sl}$ corresponding to the unit Reynolds numbers at which transition moved onto the model base for $g/d = 0.12$ and 0.16 based on the heat-transfer data. (See figs. 13 and 14.) The values of $R_{\theta,w,sl,T}$ for $g/d = 0.16$ and from the corrected curve for $g/d = 0.12$ are 390 and 360, respectively. No δ^* correction was included for $g/d = 0.16$ because for this large gap at the high Reynolds number at which transition was observed, the effect of the correction was expected to be small. Also shown in the figure are $R_{\theta,w,sl}$ levels above which transition would be expected to occur based on the criteria of reference 14. The calculated values for the rod model are much higher than these levels, probably because levels from reference 14 are based on subsonic data at low to moderate sweep angles.

If the $R_{\theta,w,sl}$ values of 360 to 390 represent a preliminary "correlation" for transition, then an estimate based on trends from figure 16(a) indicates, for example, that transition should occur at $R_\infty \approx 29 \times 10^6$ per m (9×10^6 per ft) for $g/d = 0.2$. Thus, a 25-percent increase in gap size (from $g/d = 0.16$ to 0.2) may increase transition Reynolds number by about 30 percent. The benefits from this possible increase in transition Reynolds number, which would have to be verified by further tests, would be at the expense of an increase in suction mass flow of about 25 percent for a wind-tunnel sound shield. (See ref. 15.)

Figure 16(b) presents a plot of the stagnation-line momentum thickness Reynolds number against the measured transition length Reynolds number for $g/d = 0.16$ and 0.12. The data points for the present investigation are the transition values of $R_{x,T}$ at the corresponding values of R_∞ (fig. 13) which are then used to enter figure 16(a) to obtain $R_{\theta,w,sl,T}$. Also shown in figure 16(b) are subsonic data for a 45^o swept, blunt-leading-edge wing (ref. 16) with and without suction through chordwise slots. Although the present rod model and the wing of reference 16 are entirely different configurations and were tested at different Mach numbers, the effect of suction on the wing and the effect of increasing the gap width of the rod model are similar in that the levels of $R_{x,T}$ are increased for both configurations with little change in $R_{\theta,w,sl,T}$. In view of the large dif-

ferences in Mach number and flow geometry of the two experiments, it is encouraging that the values of $R_{\theta,w,s\ell,T}$ are not too different. These two results suggest that the general characteristics of the flow for the two experiments are probably similar.

In summary, figures 13 to 16 illustrate the severe reduction in the transition Reynolds number obtained on the rod model as the gap width is reduced. Hence, it may be concluded that a wind-tunnel sound shield utilizing 0.635-cm-diameter (0.25-in.) rods should be designed with 0.102-cm (0.040-in.) gaps. Larger capacity vacuum ducts will then be required to handle the higher mass flows than would have been possible with the smaller gap widths.

Fluctuating Pitot Pressure Measurements

In order to determine the effectiveness of the rod model for shielding a flow field from radiated noise, it is necessary to know the maximum possible noise reduction for an ideal sound shield. Laufer (ref. 17) suggested that the total sound intensity (mean square of pressure fluctuations $(\tilde{p})^2$) in a high Mach number wind tunnel with a square test section is composed of approximately equal contributions of direct radiated noise from the turbulent boundary layer on each of the four nozzle walls and there would be little or no reflection of sound from opposite tunnel walls. In order to verify this effect, Laufer measured the noise intensity $(\tilde{p})^2$, in the free stream due to a tripped turbulent boundary layer on only one wall when the other walls were laminar. This measured intensity was approximately one-fourth of the mean square intensity measured when all four tunnel walls were turbulent. Hence, it appears that there are equal contributions of direct radiated noise from each of the four tunnel walls and that no correlation between them exists. That is, the rms pressure fluctuations from one wall would be equal to one-half that of the total from four walls.

The rod model is planar and is mounted approximately on the tunnel center line (see fig. 3); therefore, by following Laufer's reasoning (ref. 17), the model can at best shield a probe mounted within its "shadow zone" from approximately one-half the total noise intensity generated by the turbulent boundary layers on the tunnel walls. This statement assumes that the contributions of all four walls are equal. It also assumes that the present model would provide the same noise shielding as an ideal flat plate (no noise reflection or generation by the plate) that spans the tunnel. The reductions in tunnel rms pressure levels were determined by first normalizing the net pressure level measured within the rod model flow field by the measured local mean pitot pressure. These normalized rms pressure fluctuation levels in the flow field of the model expressed as ratios with the corresponding normalized levels in the free stream are presented in figure 17. This figure shows that when the rod boundary layers were laminar, the rod model with $g/d = 0.16$ reduced the normalized rms pressure levels by about 45 percent. For $g/d = 0.068$

and 0.12, the rms pressure levels were reduced by about 40 percent when the rod boundary layers were laminar.

The measured reductions in rms pressure levels of 45 and 40 percent correspond to decreases in mean square pressure (intensity) of approximately 70 percent and 64 percent, respectively. These reductions are larger than the 50-percent reduction in intensity (mean square of pressure fluctuation) expected on the basis of the reasoning in reference 17. The increased rms pressure reductions measured in the present experiments are probably due to asymmetry of the probe location and model position in the test section. That is, the locus of points representing the acoustic origins seen by the fluctuating pitot probe placed in the model flow field is a complex curve for a two-dimensional nozzle, particularly at a test-section Mach number of 6 and for the present model geometry. It is not clear that contributions of radiated noise from the four tunnel walls would be equal under these circumstances. Consequently, the 50-percent reduction in intensity that might be expected for an ideal flat shield is probably not applicable to the present wind-tunnel experiment. Another possible explanation for the larger attenuation in the intensity of the pressure fluctuations in the present tests as compared with the maximum theoretical 50-percent attenuation of an ideal flat shield is the interaction or refraction of the complex directional radiated sound field with the shocks, slip lines, and other nonuniform flow conditions in the model flow field. Obviously, additional experiments, probably with a hot-wire anemometer, will be needed to clarify the present results. Also, tests of an actual sound shield that completely encloses a test region (ref. 15) are required.

Another important result shown by the data for $g/d = 0.12$ in figure 16(b) is that the rms pressure level measured over a rod is only slightly higher than that measured over a gap, transition being indicated at the same unit Reynolds number. Thus, except for unknown "edge" effects, the rms pressure field should be essentially uniform within the shielded region of a sound shield.

For each gap size there is a pronounced increase in the rms pressure level when a certain unit Reynolds number is reached. (See fig. 17.) This increase in the rms pressure level is caused by transition of the boundary layers on the rods at the acoustic origin of the disturbances sensed by the probe. There is a significant decrease in this unit Reynolds number for transition when the gap width is reduced.

Transition Reynolds numbers were calculated from the rms pressure measurements by using the distance from the leading edge of the model to the acoustic origin and the unit Reynolds numbers at which the rms pressure levels began to increase rapidly from the lowest levels indicated in figure 17. These results are presented in figures 13 and 14 and show that the transition length Reynolds numbers and x_T values from the pitot probe data are significantly lower than those obtained from the heat-transfer rates for $g/d = 0.068$ and 0.12. The reason for this difference is believed to be due to the fact that

transition occurred around the rods before moving onto the stagnation line. The thermocouples at the stagnation line would not sense transition off the stagnation line, but the probe would. That is, this behavior of transition for the smaller gap settings would suggest that the spreading angle for turbulence is such that the effects of turbulence moved downstream from $x = 24.64$ cm (9.7 in.) and $\phi = 90^{\circ}$ to $x = 60.96$ cm (24 in.) and $\phi = 0^{\circ}$ as its effect propagated downstream and around the rods.

For $g/d = 0.16$, the transition Reynolds numbers and x_T values based on the fluctuating pitot pressure data are only slightly smaller than those from the heat-transfer data. Thus, for the largest g/d value, transition appears to move forward rapidly from the model base, more in accordance with expected transition behavior on a swept cylinder without tip effects.

Noise Spectra

Examples of spectra obtained with the pitot probe located in the flow field of the rod model with $g/d = 0.16$ and with the model at an angle of attack of 10° (ref. 6) are shown in figures 18. For the data in figure 18(a) the boundary layers on the rods were laminar. The shape of the spectra in the flow field of the model and tunnel free stream are similar, peak output occurring at low frequencies. This shape is similar to those obtained when the boundary layer on the tunnel wall is turbulent. This result suggests that when the flow on the rods is laminar, the rms pressure levels in the model flow field are dominated by the turbulent boundary layer on the nozzle wall. The spectra for a local unit Reynolds number of 42.7×10^6 per m (13×10^6 per ft) are shown in figure 18(b). There is a general increase in the noise level in the model flow field. This increase is especially pronounced at frequencies above 55 kHz. The shape of the curve suggests that the flow on the rods is not yet a fully developed turbulent boundary layer which would presumably radiate noise only at very high frequencies.

Figures 19(a), 19(b), and 19(c) show spectra for $g/d = 0.068$ and 0.12 when the boundary layer on the rods was laminar. The trends for these gap spacings are similar to those for $g/d = 0.16$ when the boundary layer on the model was laminar. Also, the spectra measured in the flow field of the model and those measured in the free stream (fig. 19(d)) are very similar and indicate that when the boundary layer on the model was laminar, there were apparently no significant extraneous pressure disturbances generated by the rod model that entered the semishielded region.

Spectra measured when the pitot probe was over a gap (fig. 19(b)) and over a rod (fig. 19(c)) indicate that the spectral distribution of the noise is uniform across this portion of the span of the model. Therefore, the slight increase in the level of the noise measured over a rod (fig. 17) is due to a general increase of the noise level at all frequencies.

CONCLUSIONS

A 0.61-m long (2-ft) planar sound shield model was tested in the Langley Mach 6 20-inch tunnel. The model consisted of 0.635-cm-diameter (0.25-in.) rods that were almost alined with the local flow direction with gaps between the rods for boundary-layer removal. Data were obtained for three different gap settings corresponding to ratios of gap width to rod diameter (g/d) of 0.16, 0.12, and 0.068. Tests were conducted over a local unit Reynolds number range from 3.3×10^6 to 42.6×10^6 per m (1.0×10^6 to 13.0×10^6 per ft). The ratio of wall temperature to free-stream total temperature was about 0.62. The model was tested at angles of attack of 5^o and 10^o.

In general, the most important factors involved in the design and performance of a supersonic wind-tunnel sound shield are the rod diameter, gap width, unit Reynolds number, and design of the leading-edge fairing and rod support structure to minimize flow disturbances. Also, it is important to determine whether any pressure recovery of the supersonic flow in the gap can be realized since the cost of the vacuum ducting system could then be reduced and the tunnel run time could be increased.

Specific conclusions are as follows:

1. Fluctuating pitot-pressure measurements showed that a 45-percent reduction of the normalized root-mean-square (rms) pressure level was obtained with a g/d of 0.16. This large size gap requires large vacuum capability. Smaller gap sizes were therefore tested since the suction mass flow requirements for a wind-tunnel sound shield would thereby be reduced. The results indicate that the smaller gaps (g/d = 0.12 and 0.068) provided at most a 40-percent reduction of the normalized rms pressure level when the boundary layers on the rods were laminar. These measured reductions in rms pressure levels are larger than the theoretical possible maximum of about 30 percent that would be expected for an ideal flat plate mounted at the tunnel center line and spanning the test section. The reasons that the measured reductions are larger than the theoretical value are possibly related to asymmetrical probe and model locations in the tunnel or to reflection and refraction effects on the tunnel sound field of the model shock and flow field.

2. The maximum transition Reynolds number was substantially reduced as gap size was reduced. This reduction in the transition Reynolds number is believed to be due to viscous effects which restrict the flow through the gaps. Transition behavior for g/d = 0.068 bears a strong resemblance to the behavior of transition on a flat plate. For the largest gap, however, the maximum transition Reynolds numbers approach those obtained on isolated swept cylinders with root disturbances. Hence, this largest gap width may be close to the minimum size needed to obtain this swept cylinder behavior. Thus, larger vacuum capacities are required for a wind-tunnel sound shield application than would be possible with the smaller gaps.

3. A comparison of transition Reynolds numbers as indicated by the fluctuating pitot probe and by the measured heating rates indicates that for g/d ratios of 0.068 and 0.12, transition first occurs off the stagnation line and spreads downstream and around the rods to the stagnation line. For $g/d = 0.16$, transition moves abruptly forward from the model base and the corresponding transition Reynolds numbers based on the two different techniques are in close agreement. Even though the transition behavior is different for the two gap width-diameter ratios of 0.12 and 0.16, the "spanwise" momentum thickness Reynolds numbers at the rod stagnation lines are nearly the same when transition moves onto the model base.

4. The uniformity of the mean flow above the rods appears to be good except in the region within 1 rod diameter of the top of the rods where the flow may be influenced by vortices caused by the flat plate to round rod fairing region. Optimization of this fairing region may improve the flow uniformity and increase transition Reynolds numbers.

5. Boundary-layer calculations show that viscous effects become significant at lower unit Reynolds numbers for the small gaps. These viscous effects cause a smaller percentage of sonic cross flow to occur at the geometric minimum. However, if the lee side pressure is sufficiently low, more sonic flow can be obtained by expansion of the flow downstream of an aerodynamic minimum. Results indicate that inviscid sonic flow at the geometric minimum was obtained for $g/d = 0.16$ at an angle of attack of 10°. Lee side pressure data for the two smaller gaps indicate that expansion to inviscid sonic flow occurred at an effective aerodynamic minimum downstream of the geometric minimum for angles of attack of 5° and 10°.

6. Calculations indicate that if normal-shock pressure recovery of the supersonic flow through the gaps could be obtained, vacuum manifold pressures for a wind-tunnel sound shield could be increased to levels as much as 10 times higher than stream static pressure and still maintain inviscid sonic cross flow at the gaps. Although viscous mixing losses on the lee side of the rods will probably limit the actual pressure recovery, large savings in vacuum duct size and cost should be possible if even a fraction of the normal-shock recovery could be realized.

7. A comparison of stagnation line heating with theoretical solutions shows that the trends of the data resemble those of the boundary-layer solutions with displacement thickness corrections, but the levels of the data are in closer agreement with solutions obtained from a strictly inviscid external flow assumption. This difference in the levels may be due to increased heating rates caused by vortices generated at the region of transition from flat plate to rod.

Langley Research Center
National Aeronautics and Space Administration
Hampton, Va. 23665
October 7, 1975

REFERENCES

1. Beckwith, I. E.: Development of a High Reynolds Number Quiet Tunnel for Transition Research. AIAA J., vol. 13, no. 3, Mar. 1975, pp. 300-306.

2. Stainback, P. C.; Anders, J. B.; Harvey, W. D.; Cary, A. M.; and Harris, J. E.: An Investigation of Boundary-Layer Transition on the Wall of a Mach 5 Nozzle. AIAA Paper No. 74-136, Jan.-Feb. 1974.

3. Laufer, John: Aerodynamic Noise in Supersonic Wind Tunnels. J. Aerosp. Sci., vol. 28, no. 9, Sept. 1961, pp. 685-692.

4. Phillips, O. M.: On the Generation of Sound by Supersonic Turbulent Shear Layers. J. Fluid. Mech., vol. 9, pt. I, Sept. 1960, pp. 1-28.

5. Pate, S. R.; and Schueler, C. J.: Radiated Aerodynamic Noise Effects on Boundary-Layer Transition in Supersonic and Hypersonic Wind Tunnels. AIAA J., vol. 7, no. 3, Mar. 1969, pp. 450-457.

6. Harvey, W. D.; Berger, M. H.; and Stainback, P. C.: Experimental and Theoretical Investigation of a Slotted Noise Shield Model for Wind Tunnel Walls. AIAA Paper No. 74-624, July 1974.

7. Harvey, William D.: Effect of Rod Gap Spacing on a Suction Panel for Laminar Flow and Noise Control in Supersonic Wind Tunnels. M. Eng. Thesis, Old Dominion Univ., May 1975. (Available as NASA TM X-68718.)

8. Goldberg, Theodore J.; and Hefner, Jerry N. (appendix by James C. Emery): Starting Phenomena for Hypersonic Inlets With Thick Turbulent Boundary Layers at Mach 6. NASA TN D-6280, 1971.

9. Hixon, Barbara A.; Beckwith, Ivan E.; and Bushnell, Dennis M.: Computer Program for Compressible Laminar or Turbulent Nonsimilar Boundary Layers. NASA TM X-2140, 1971.

10. Berger, Michael Harold: Application of Boundary Layer Theory to Suction Through Streamwise Slots in Wind Tunnel Walls. M. Eng. Thesis, Old Dominion Univ., July 1974.

11. Reshotko, Eli; and Beckwith, Ivan E.: Compressible Laminar Boundary Layer Over a Yawed Infinite Cylinder With Heat Transfer and Arbitrary Prandtl Number. NACA Rep. 1379, 1958. (Supersedes NACA TN 3986.)

12. Cary, Aubrey M., Jr.; and Morrisette, E. Leon: Effect of Two-Dimensional Multiple Sine-Wave Protrusions on the Pressure and Heat-Transfer Distributions for a Flat Plate at Mach 6. NASA TN D-4437, 1968.

13. Bushnell, Dennis M.; and Huffman, Jarrett K.: Investigation of Heat Transfer to Leading Edge of a 76° Swept Fin With and Without Chordwise Slots and Correlations of Swept-Leading-Edge Transition Data for Mach 2 to 8. NASA TM X-1475, 1967.

14. Pfenninger, Werner; and Reed, Verlin D.: Laminar-Flow Research and Experiment. Astronaut. Aeronaut., vol. 4, no. 7, July 1966, pp. 44-50.

15. Beckwith, Ivan E.; Srokowski, Andrew J.; Harvey, William D.; and Stainback, P. Calvin: Design and Preliminary Test Results at Mach 5 of an Axisymmetric Slotted Sound Shield. NASA TM X-72679, 1975.

16. Pfenninger, W.; and Bacon, J. W., Jr.: Amplified Laminar Boundary Layer Oscillations and Transition at the Front Attachment Line of a 45° Swept Flat-Nosed Wing With and Without Boundary Layer Suction. Viscous Drag Reduction, C. Sinclair Wells, ed., Plenum Press, 1969, pp. 85-105.

17. Laufer, John: Some Statistical Properties of the Pressure Field Radiated by a Turbulent Boundary Layer. Phys. Fluids, vol. 7, no. 8, Aug. 1964, pp. 1191-1197.

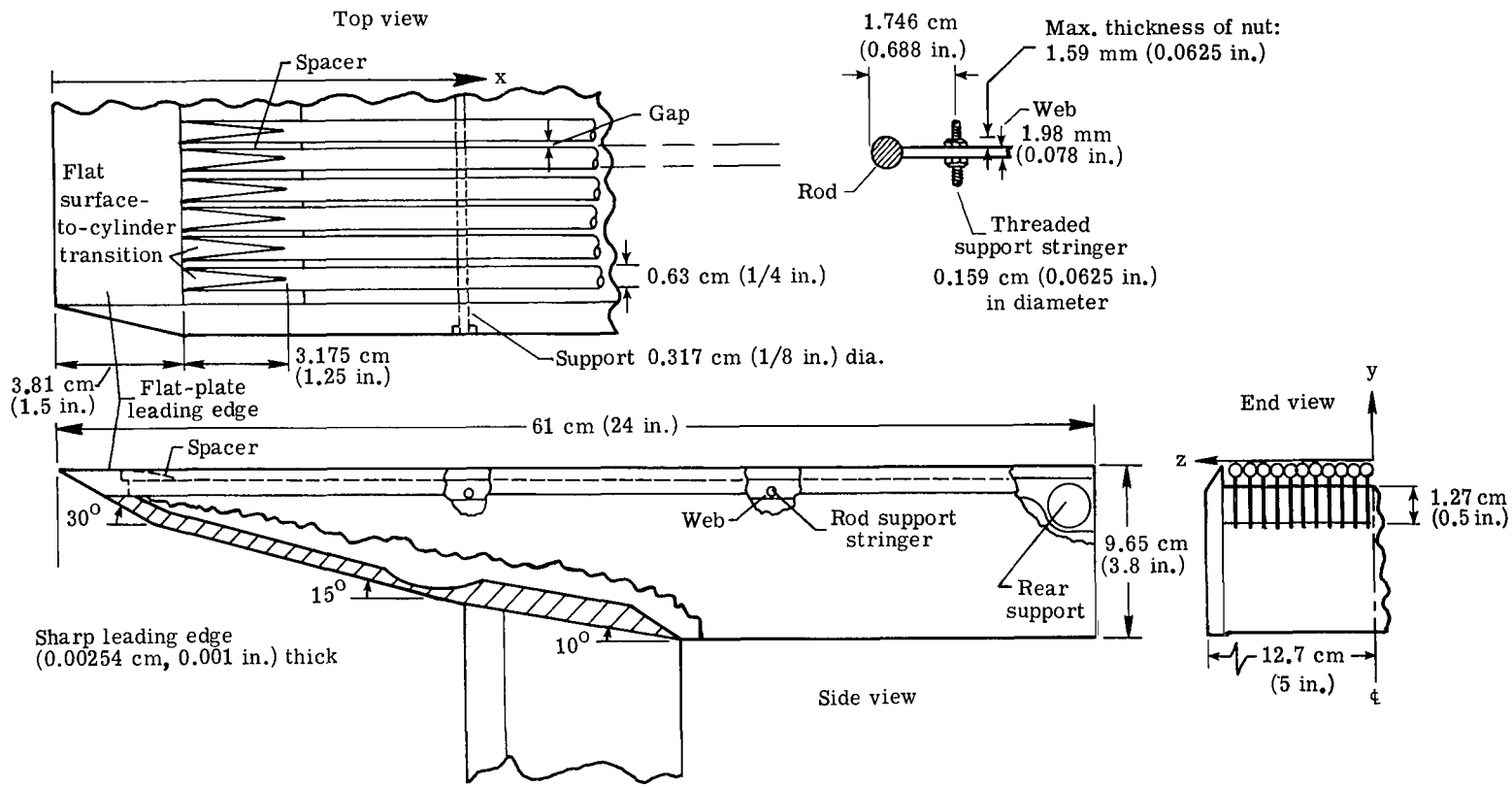

(a) Sketch of model construction details.

Figure 1.- Design and requirements for flat-plate rod model.

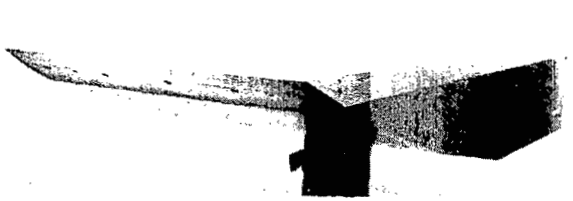

Oblique view

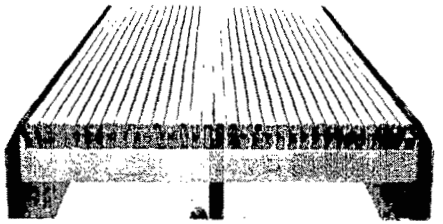

Rear view

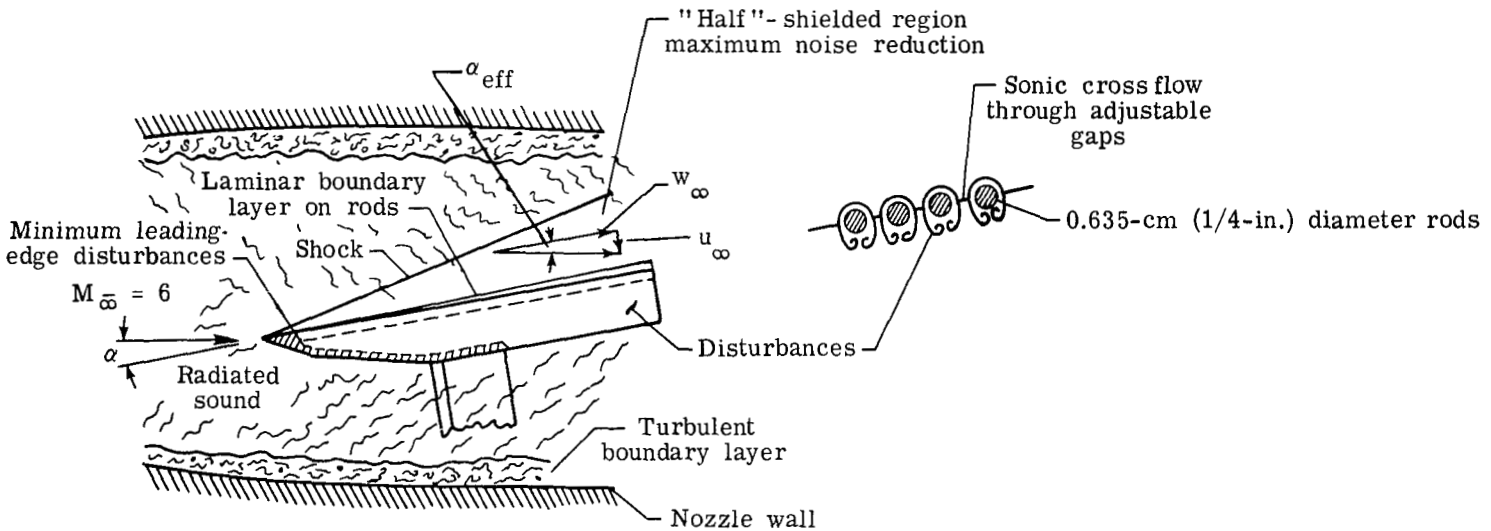

L-75-223

(b) Photograph of model and sketch of flow field.

Figure 1.- Concluded.

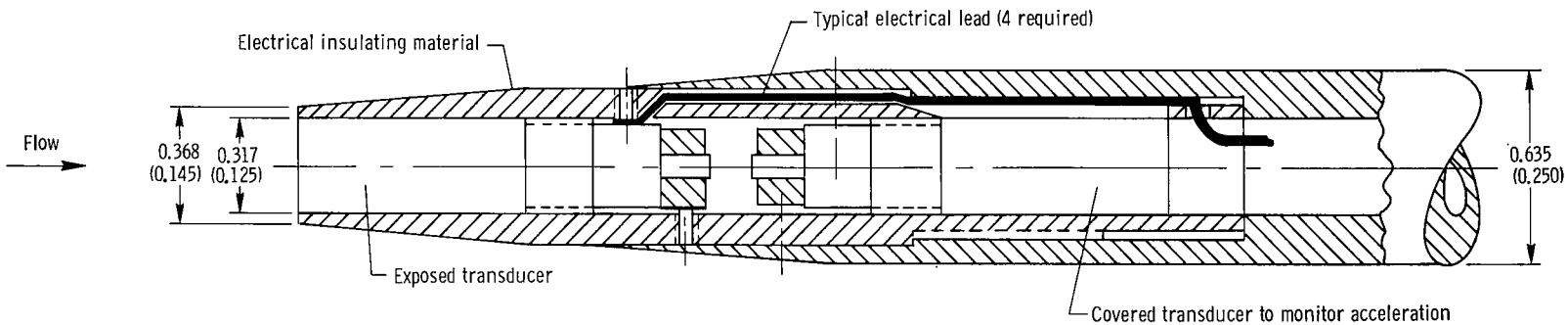

Figure 2.- Fluctuating pitot pressure probe. Dimensions are in cm (in.).

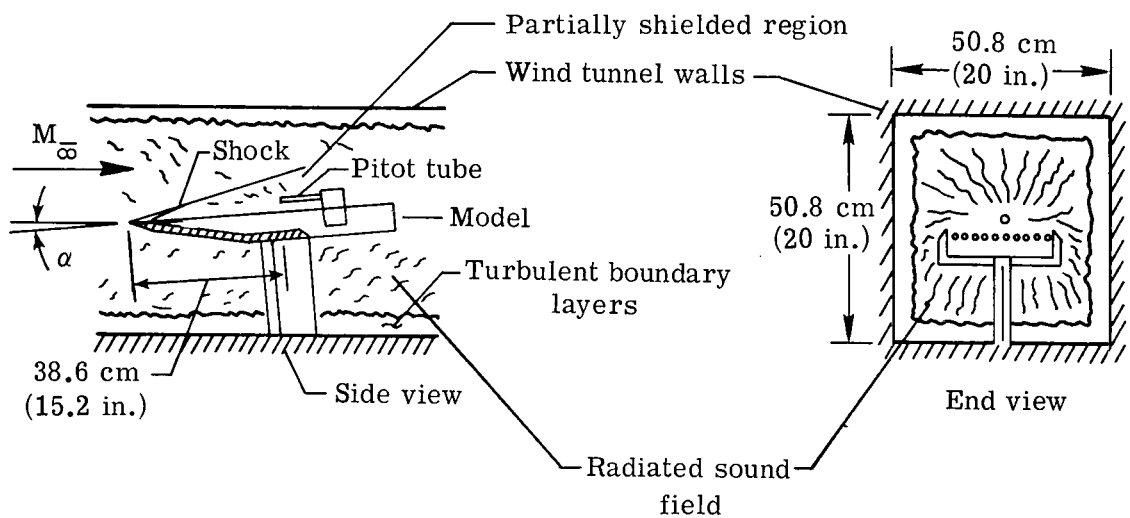

Figure 3.- Schematic view of model and idealized sound field in Mach 6 20-inch tunnel.

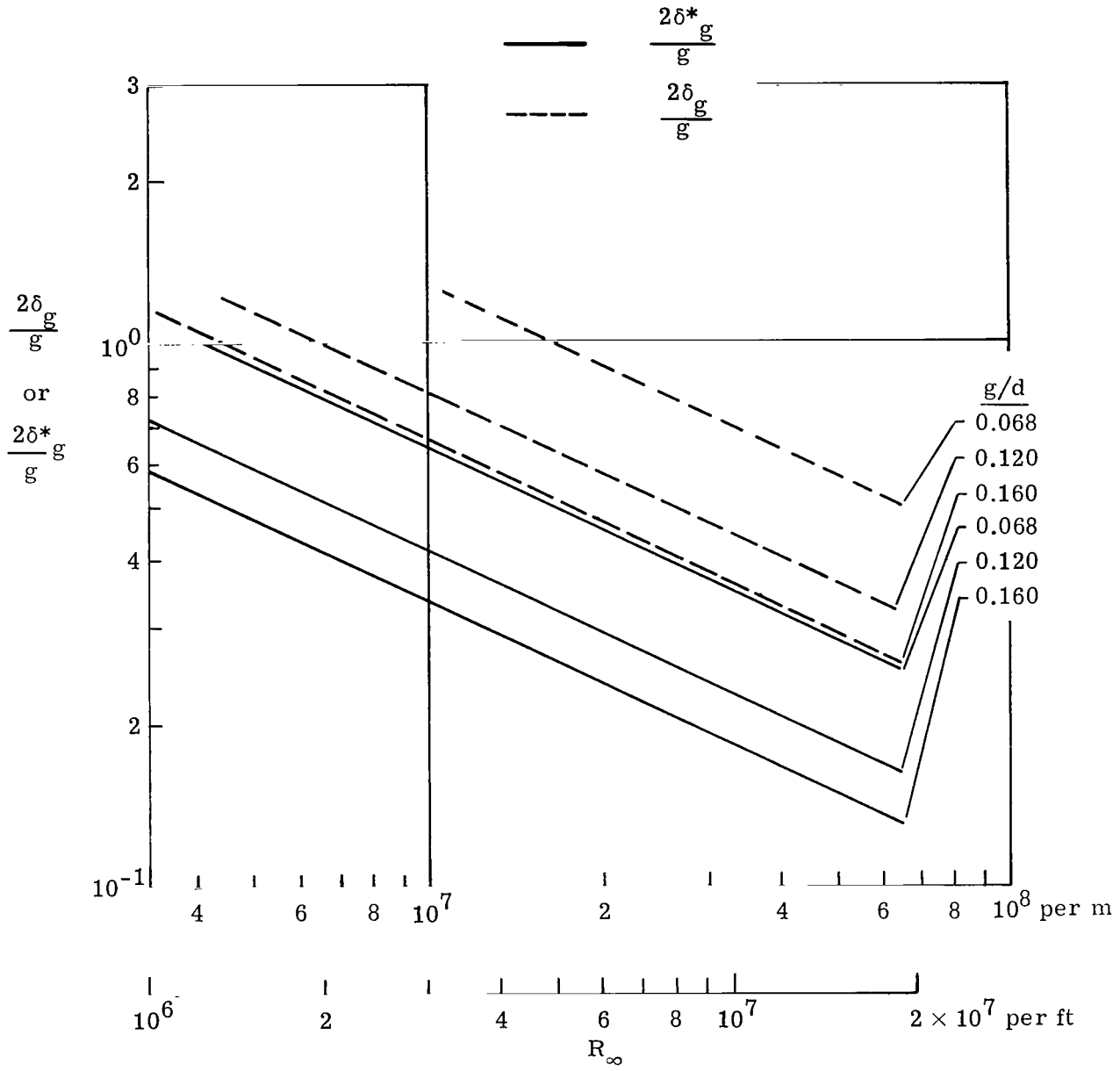

Figure 4.- Calculated laminar boundary-layer and displacement thickness at physical minimum of gap ($\phi = 90^o$). $M_\infty = 6$; $\alpha = 10^o$; d = 0.635 cm (0.25 in.).

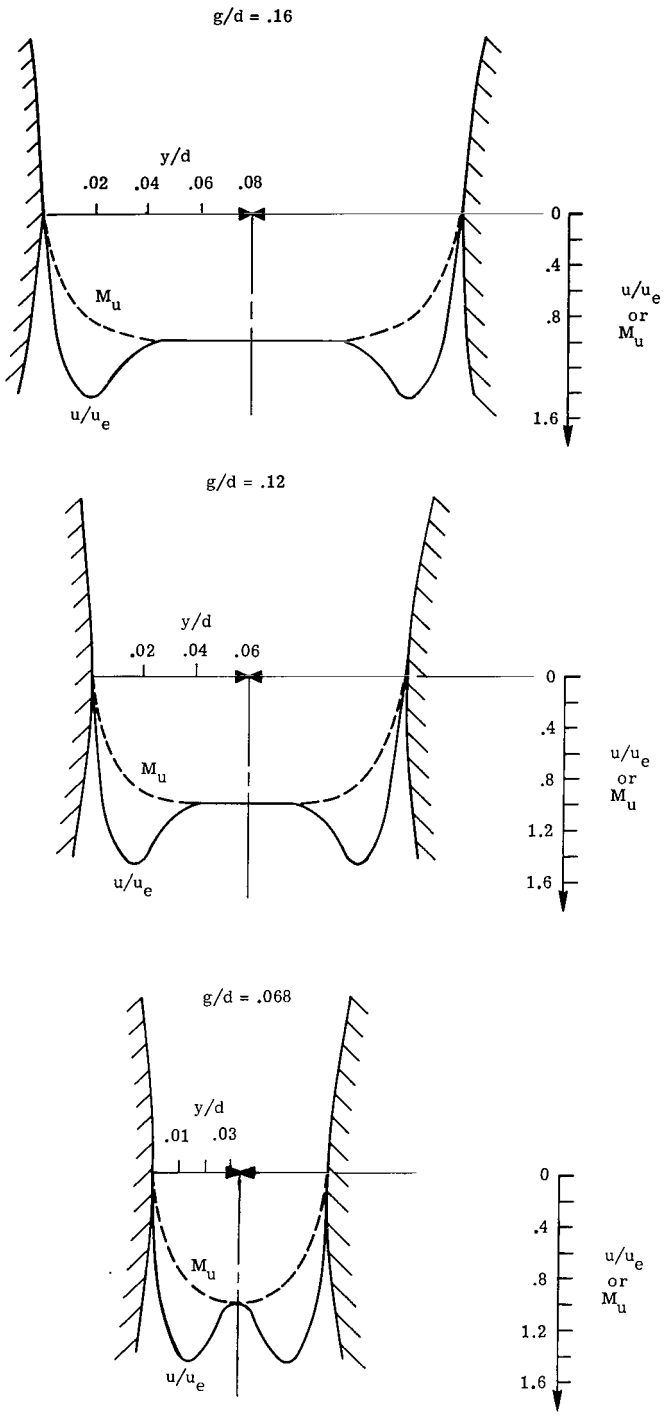

Figure 5.- Velocity and Mach number profiles in the gap.
$\phi = 90^o$; $R_\infty = 19.7 \times 10^6$ per m (6×10^6 per ft);
$\alpha = 10^o$; d = 0.635 cm (0.25 in.).

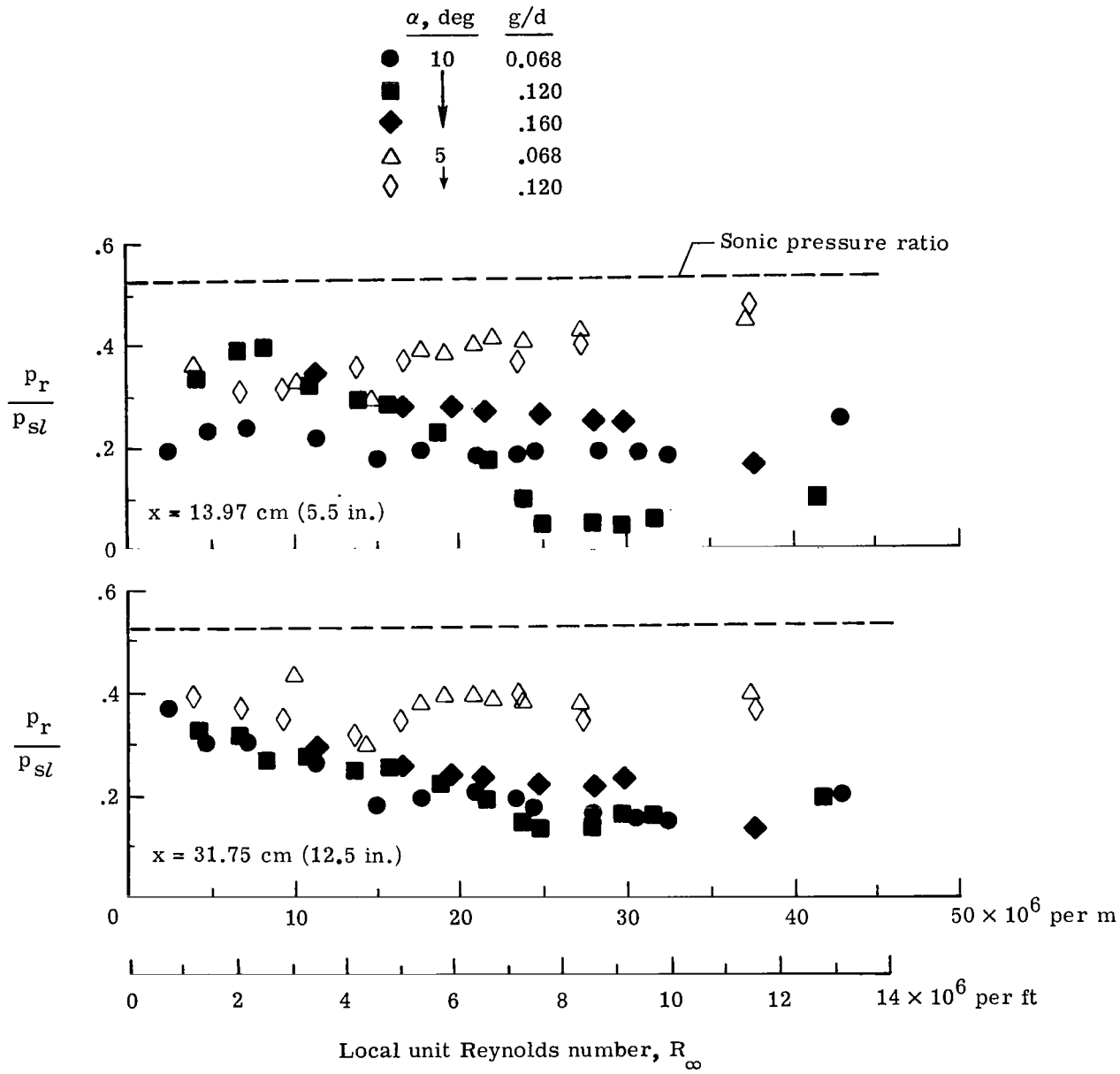

(a) Ratios of static pressure at $\phi = 180^o$ to stagnation line pressure ($\phi = 0^o$).

Figure 6.- Effect of gap spacing and Reynolds number on rod static-pressure ratios. $M_\infty = 6$; $T_{wall} = 295$ K (530^o R); d = 0.635 cm (0.25 in.).

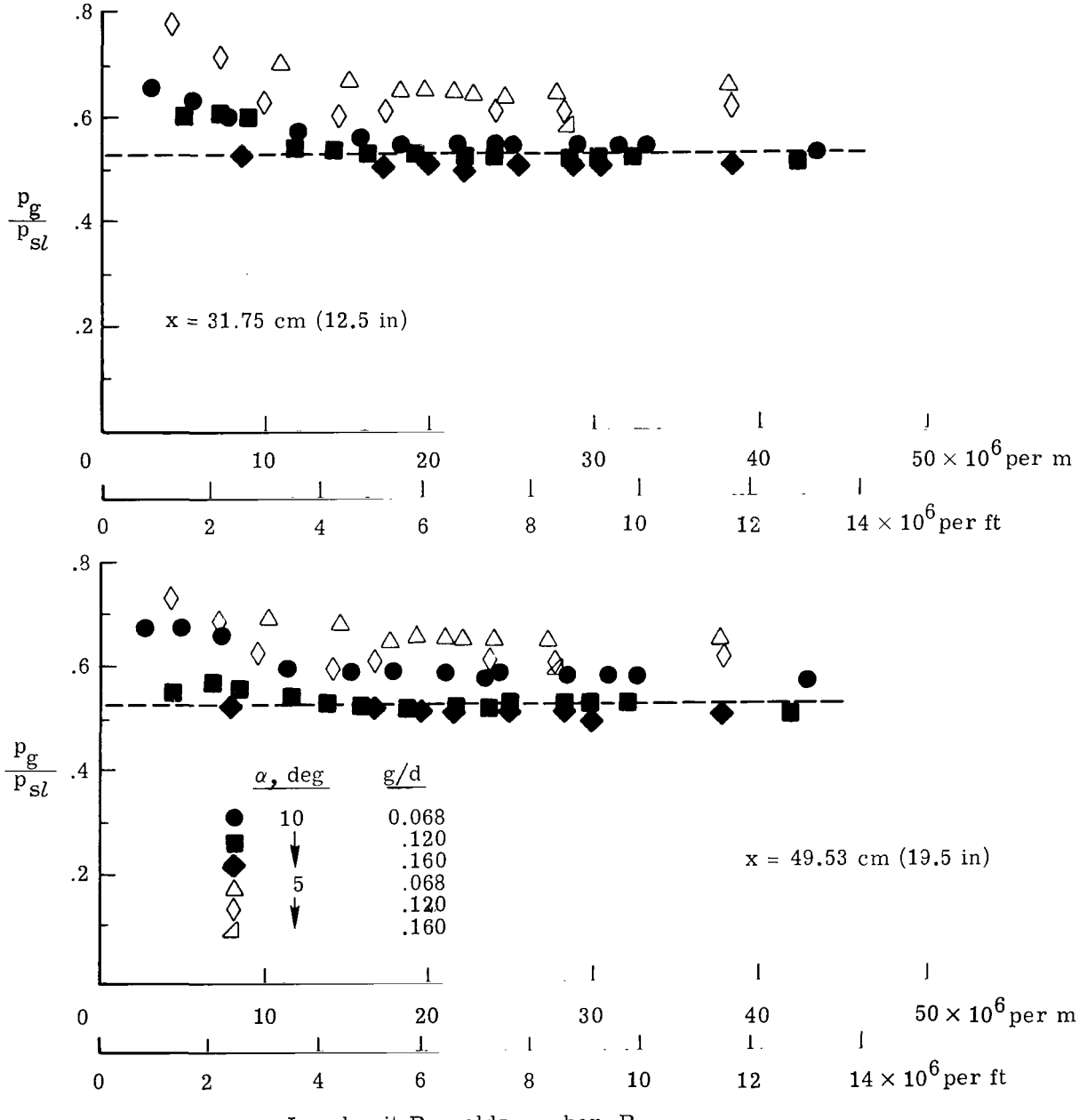

(b) Ratios of gap pressure at $\phi = 90^o$ to stagnation line pressure ($\phi = 0^o$).

Figure 6.- Concluded.

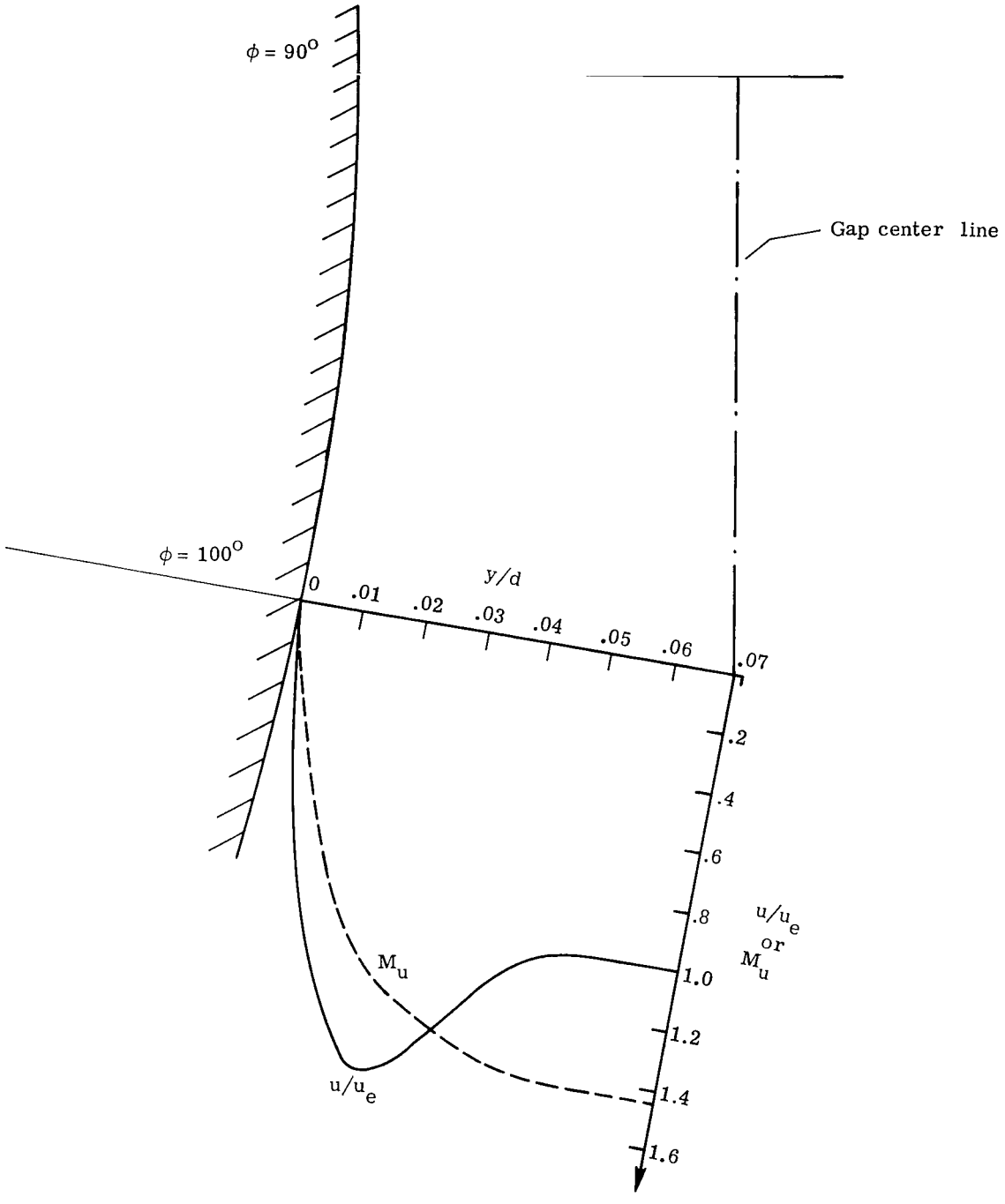

Figure 7.- Velocity and Mach number profiles at $\phi = 100^o$. $p_e/p_{sl} = 0.29$; $g/d = 0.12$; $R_\infty \approx 19.7 \times 10^6$ per m (6×10^6 per ft); $\alpha = 10^o$.

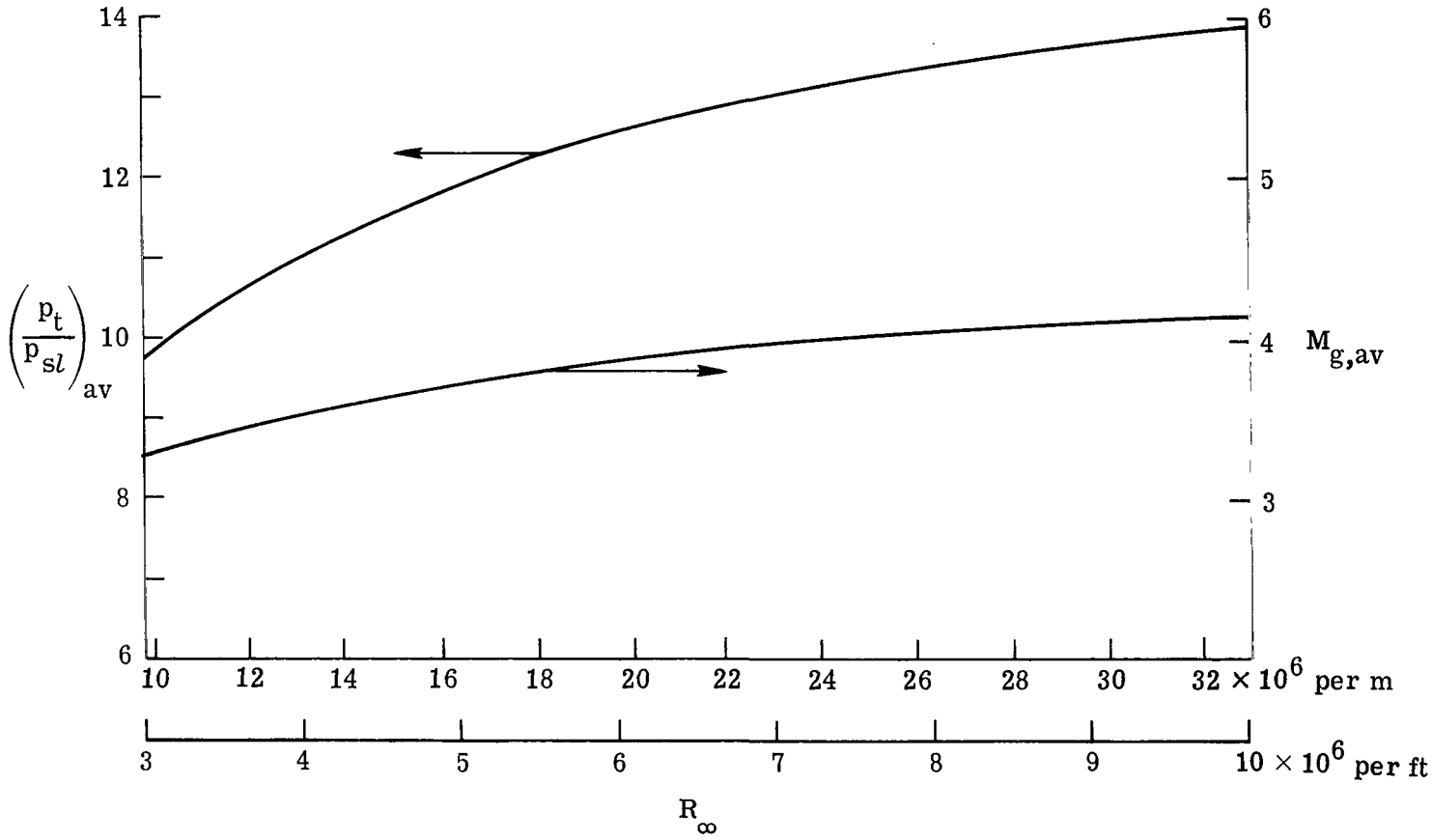

Figure 8.- Average resultant Mach number and average normal-shock pressure recovery in the gap as a function of unit Reynolds number. g/d = 0.16; $\phi = 90^o$; $\alpha = 10^o$.

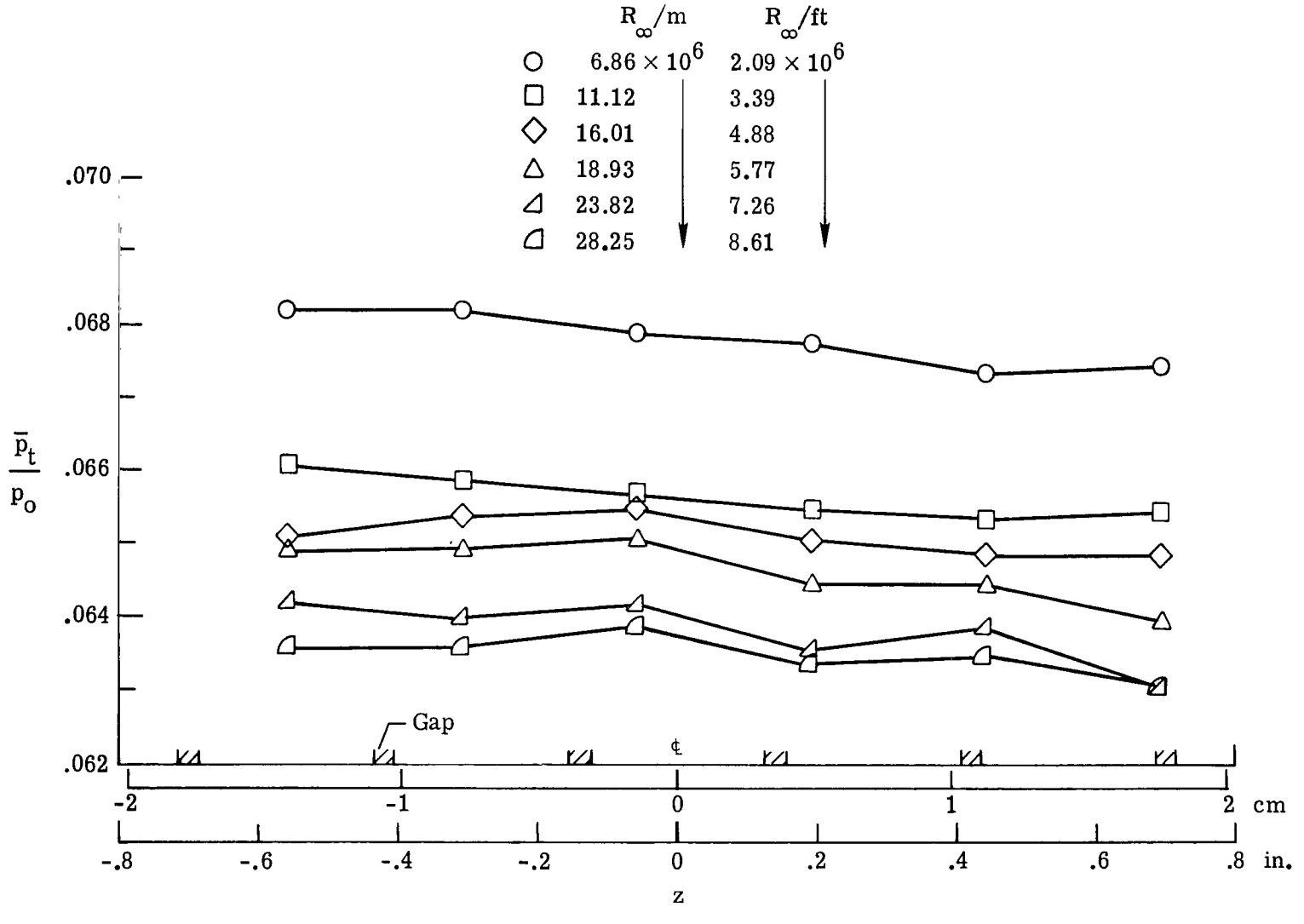

(a) Horizontal survey, y/d = 4.5.

Figure 9.- Mean pitot pressure surveys of rod model flow field for $M_\infty = 6$. $\alpha = 10^o$; g/d = 0.12; y = 2.86 cm (1.125 in.); x = 38.6 cm (15.2 in.).

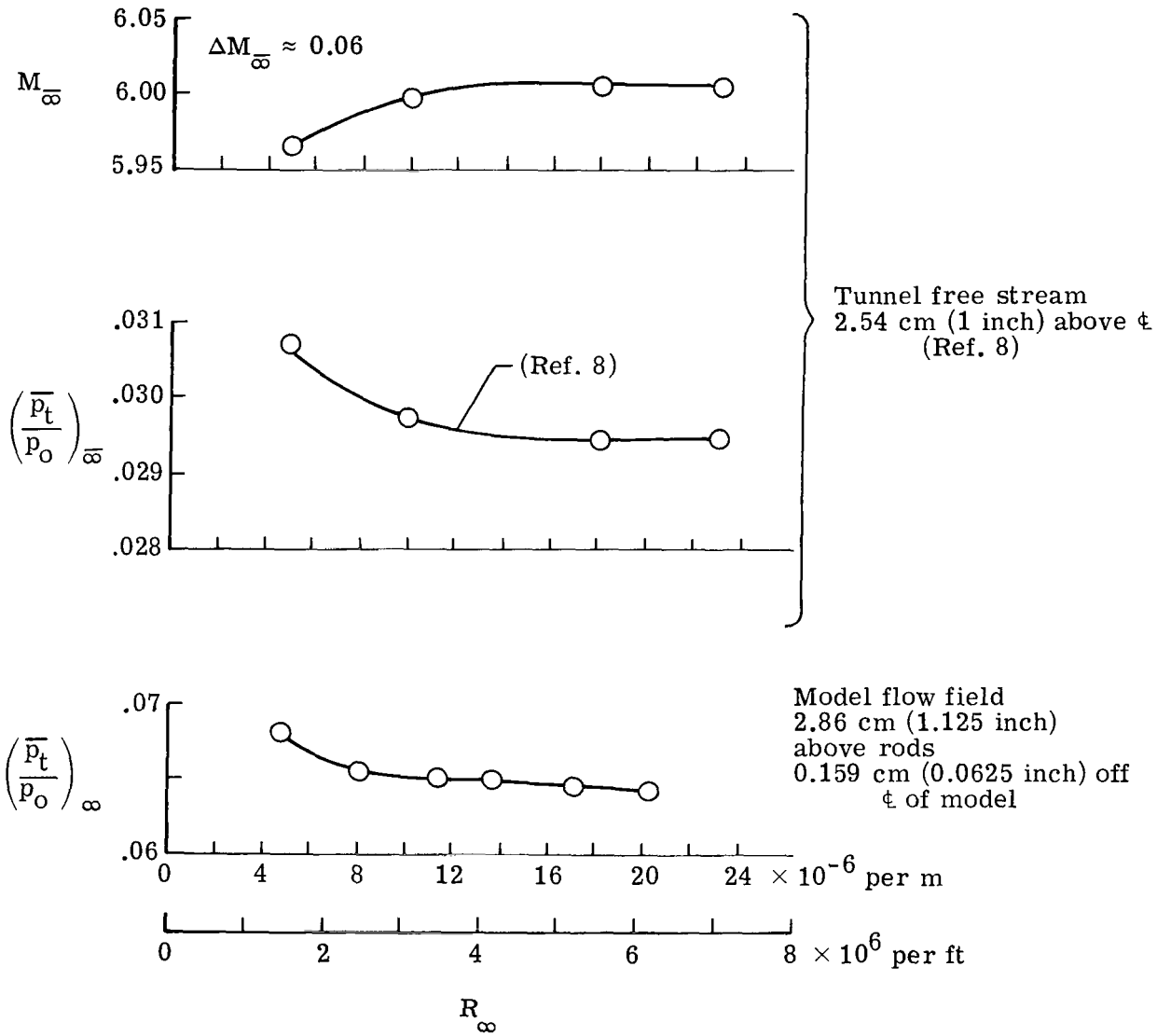

(b) Tunnel free-stream calibration.

Figure 9.- Continued.

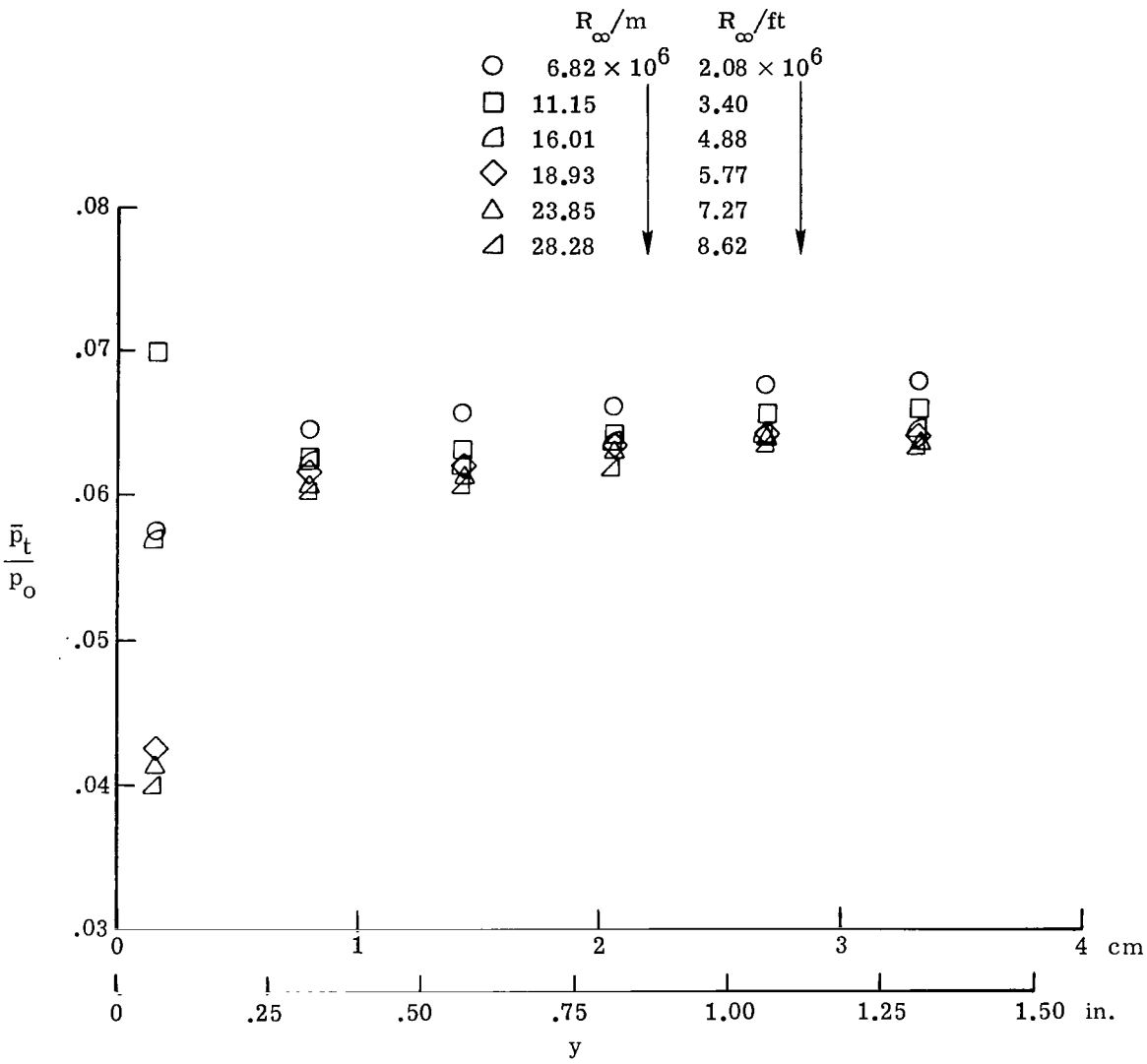

(c) Vertical survey, z = 0.

Figure 9.- Concluded.

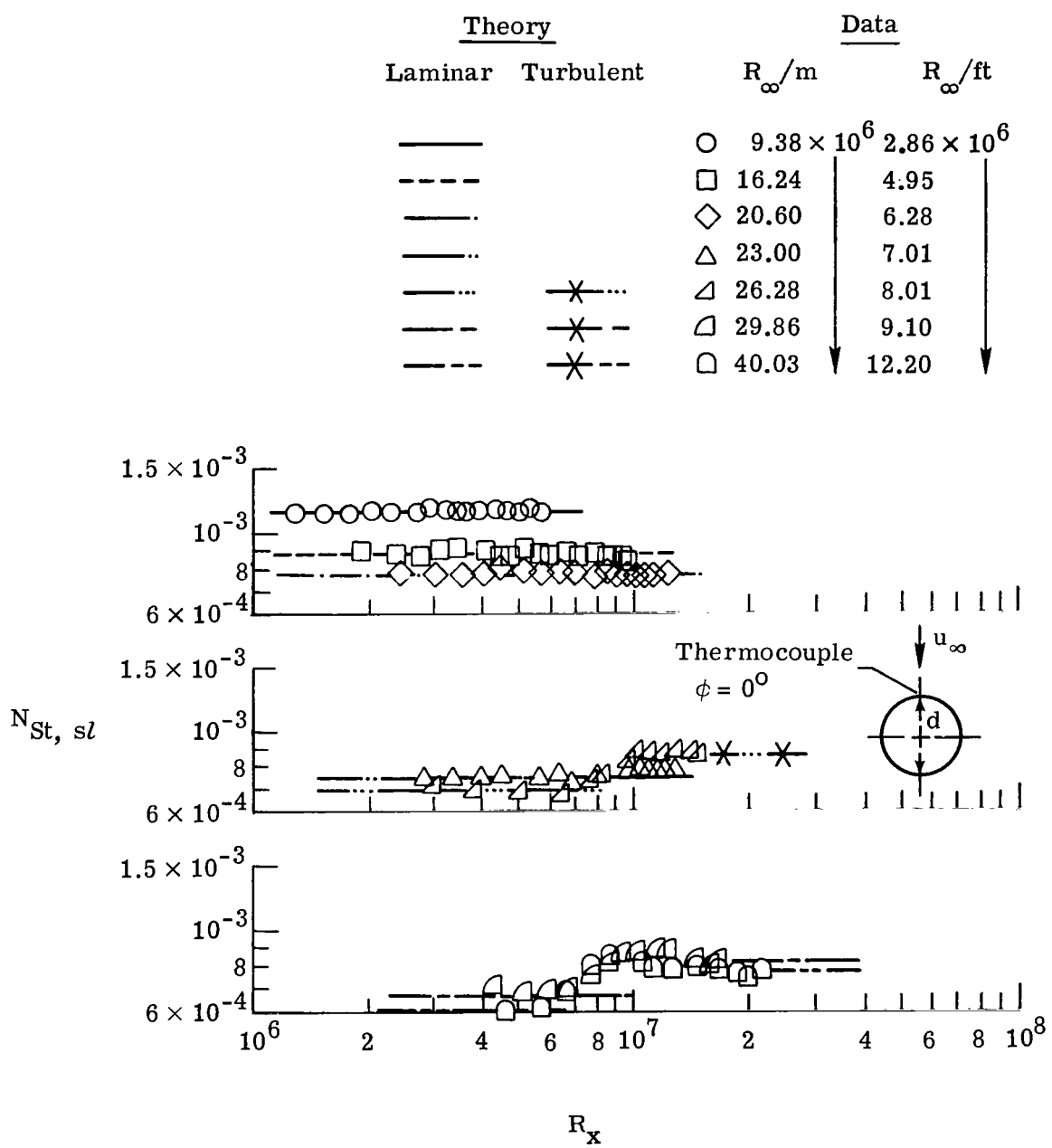

(a) g/d = 0.16.

Figure 10.- Heat transfer on windward side of rods (from ref. 6).
$M_\infty = 6$; $\alpha = 10^o$; $T_{wall} = 295$ K (530^o R).

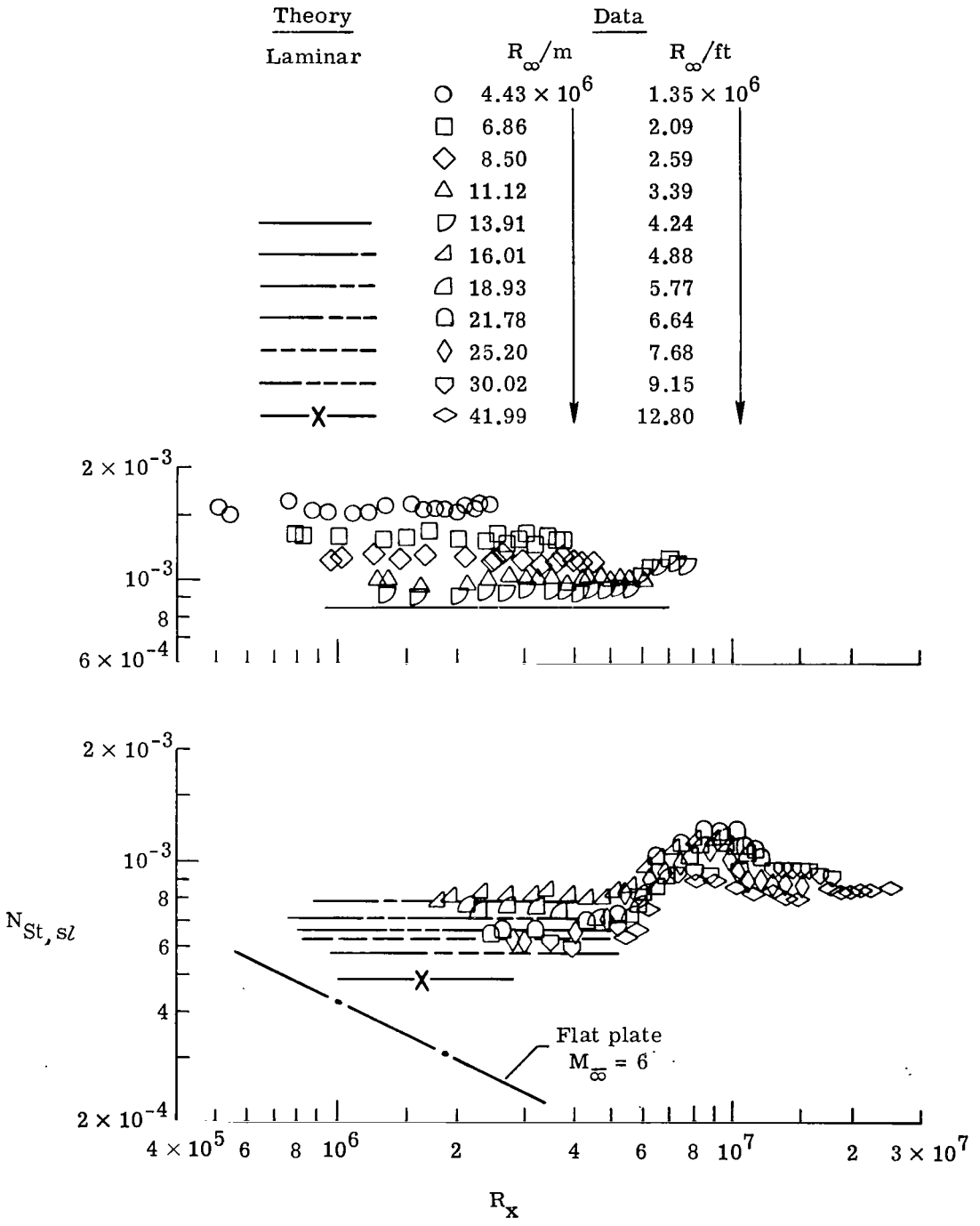

(b) g/d = 0.12.

Figure 10.- Continued.

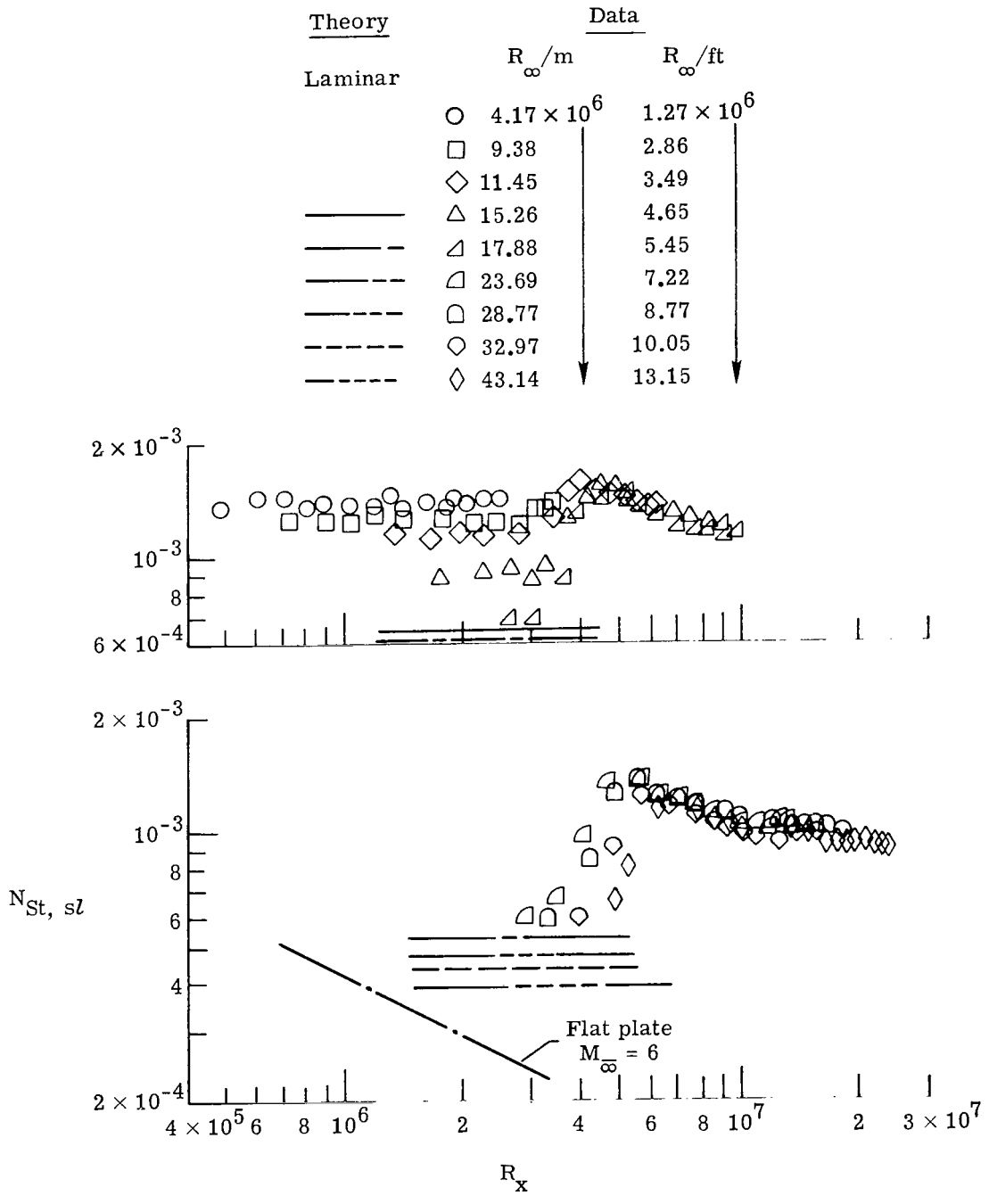

(c) g/d = 0.068.

Figure 10.- Concluded.

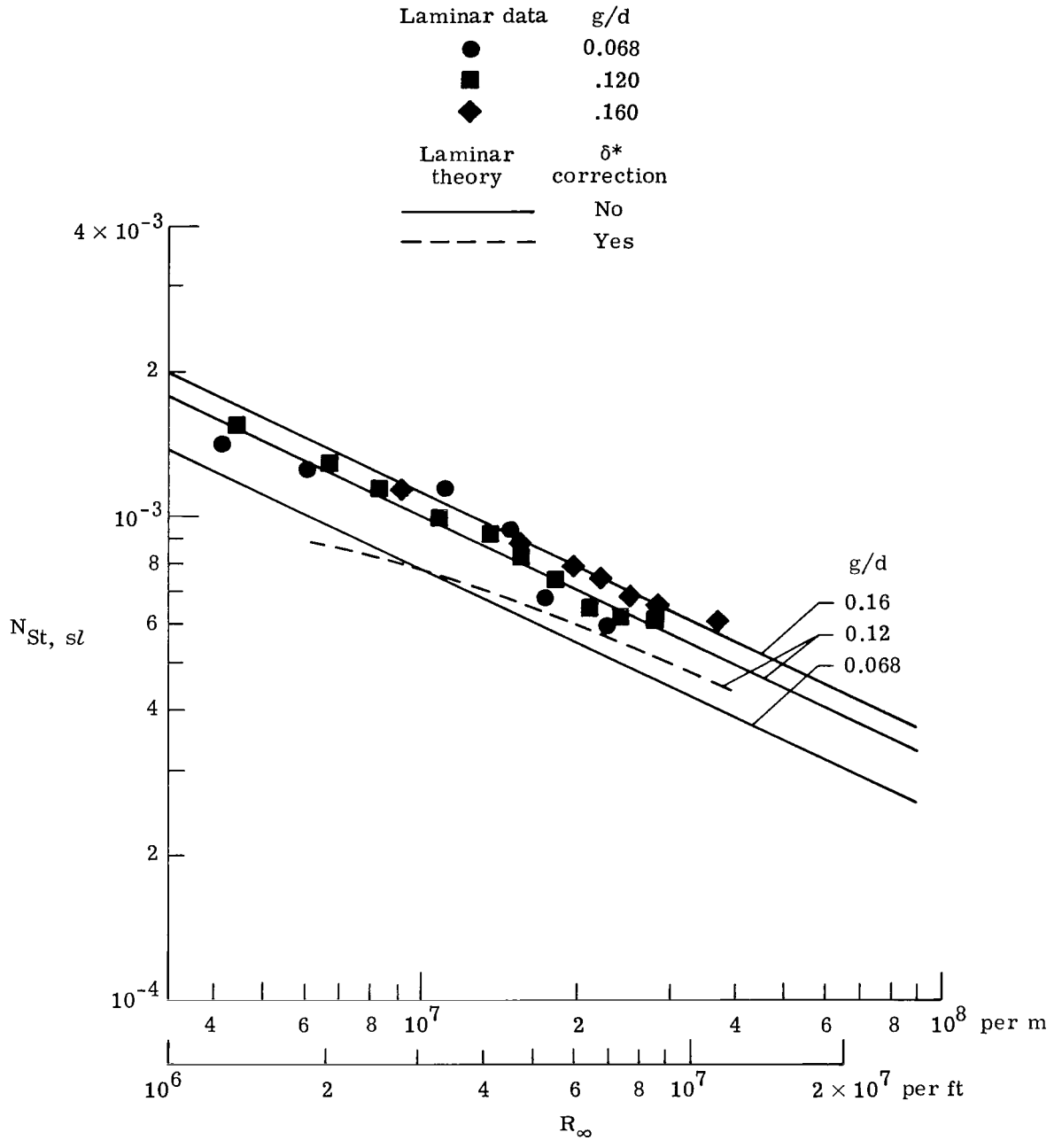

Figure 11.- Comparison of data with theory for variation of heating rate at $\phi = 0^o$ with unit Reynolds number.

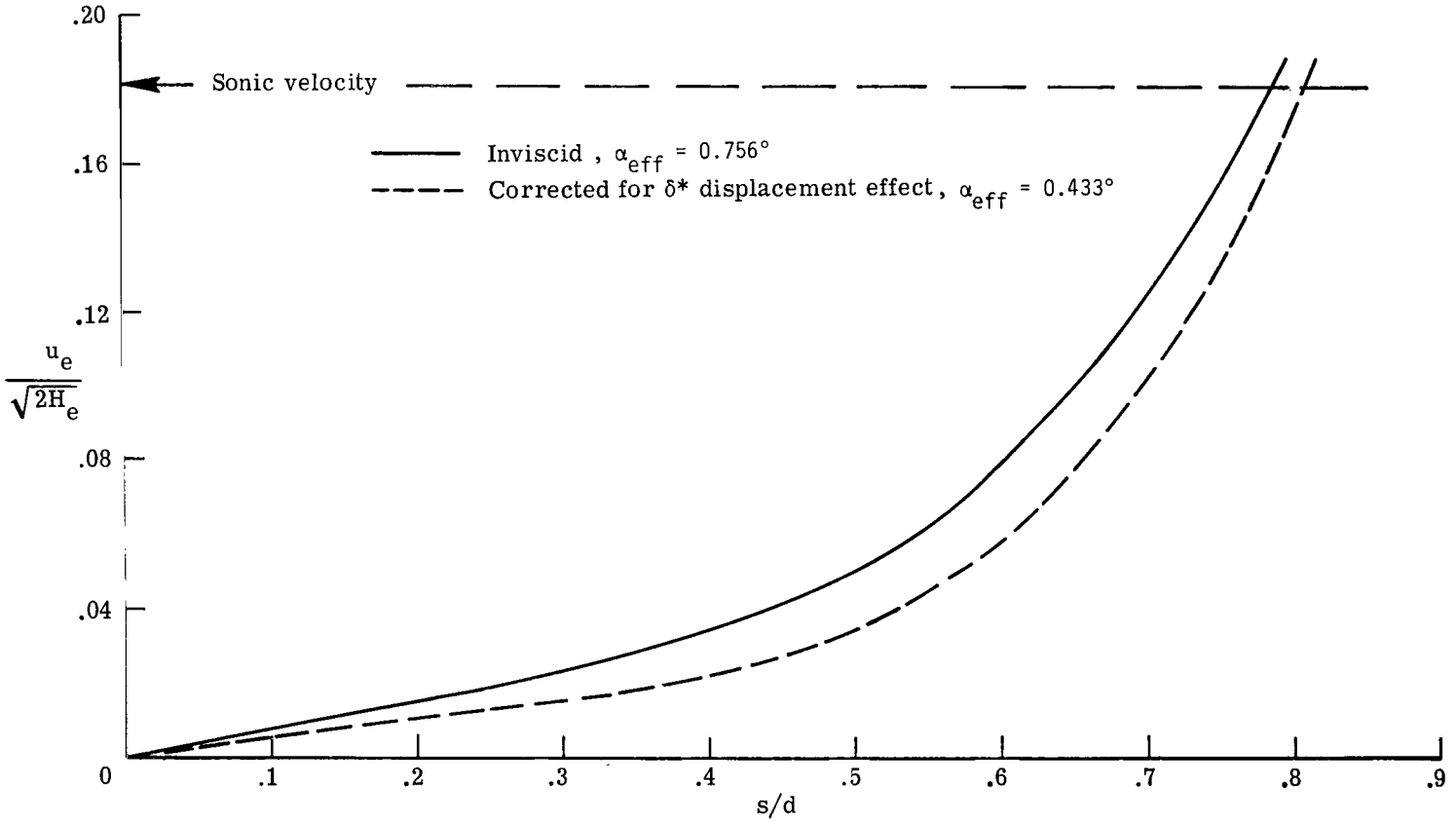

(a) Velocity distributions.

Figure 12.- Normalized streamwise velocity distributions around rods for $R_\infty = 9.84 \times 10^6$ per m (3×10^6 per ft) and stagnation-line velocity gradients as a function of Reynolds number based on rod diameter. g/d = 0.12; $\alpha = 10^o$.

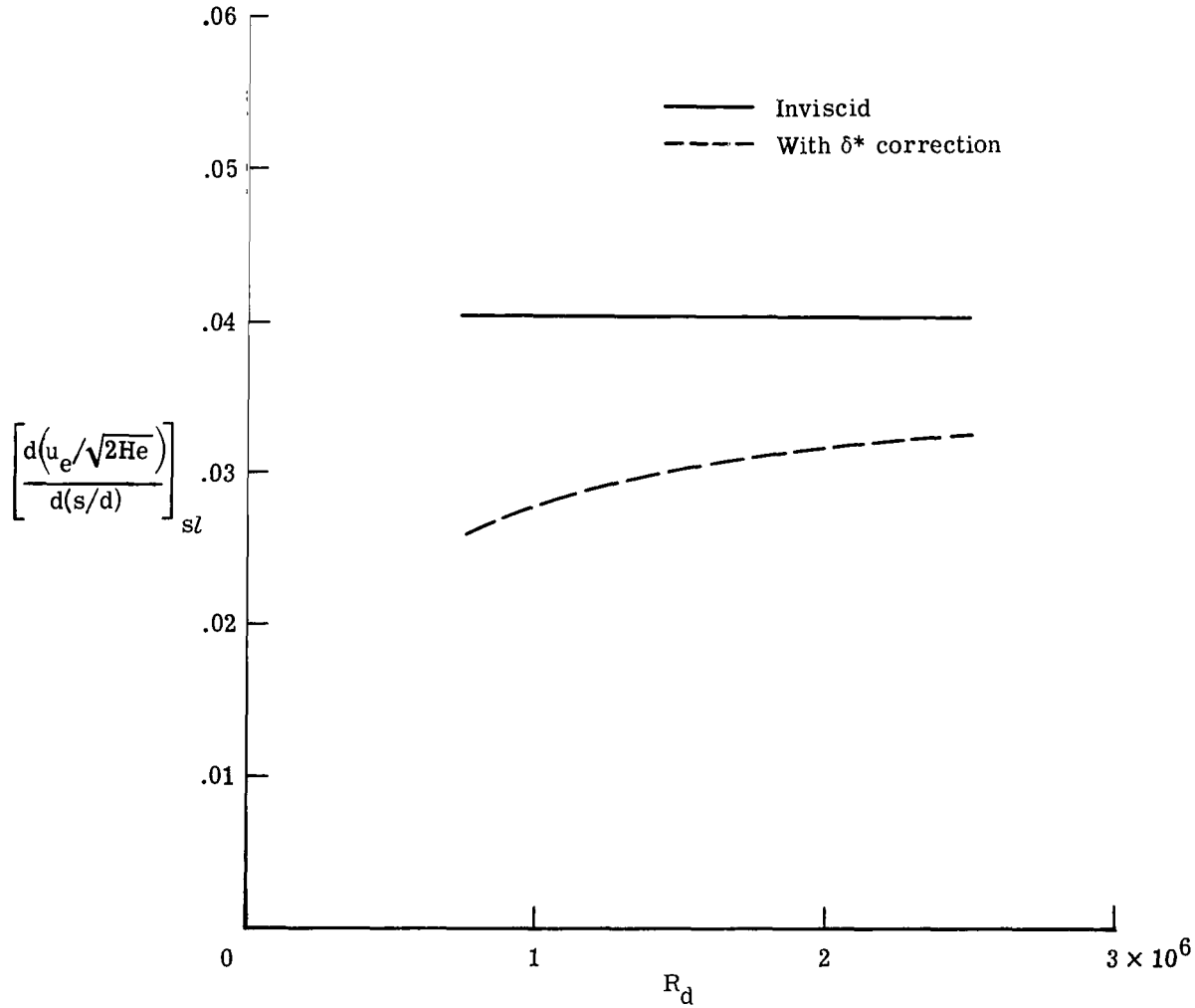

(b) Velocity gradients.

Figure 12.- Concluded.

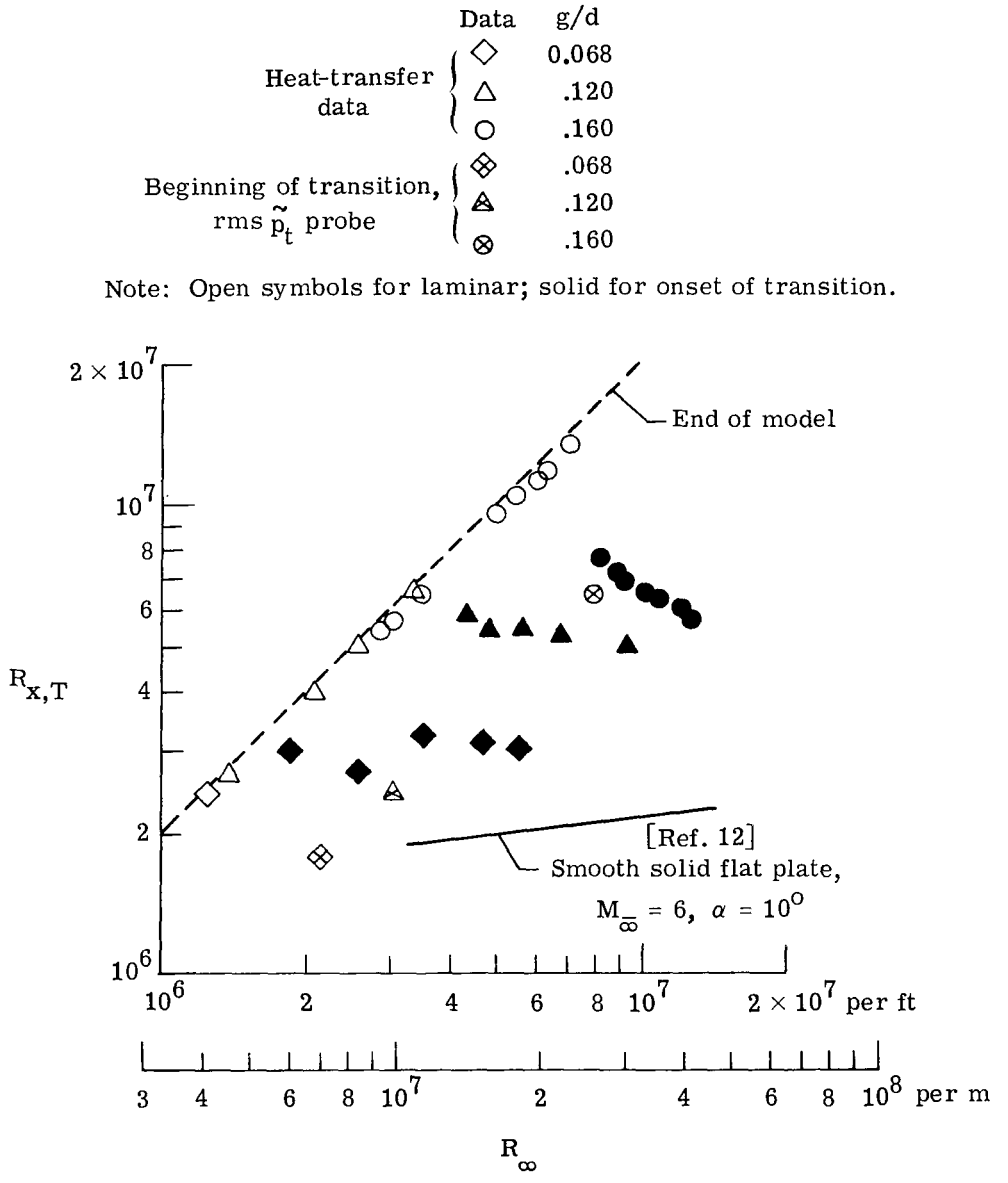

Figure 13.- Variation of transition Reynolds number with unit Reynolds number at various gap spacings. $\alpha = 10^o$.

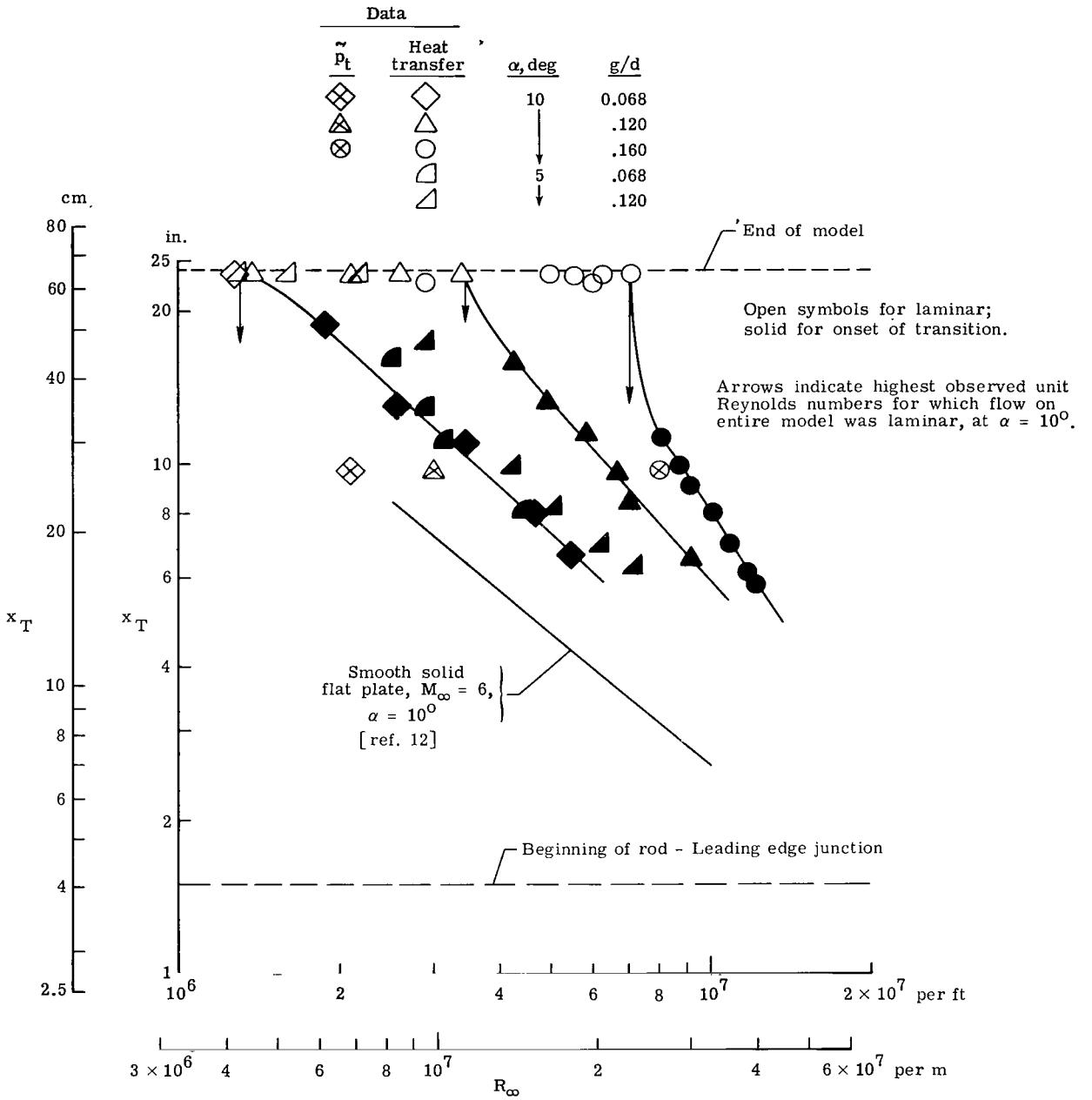

Figure 14.- Effect of gap spacing and local unit Reynolds number on transition location.

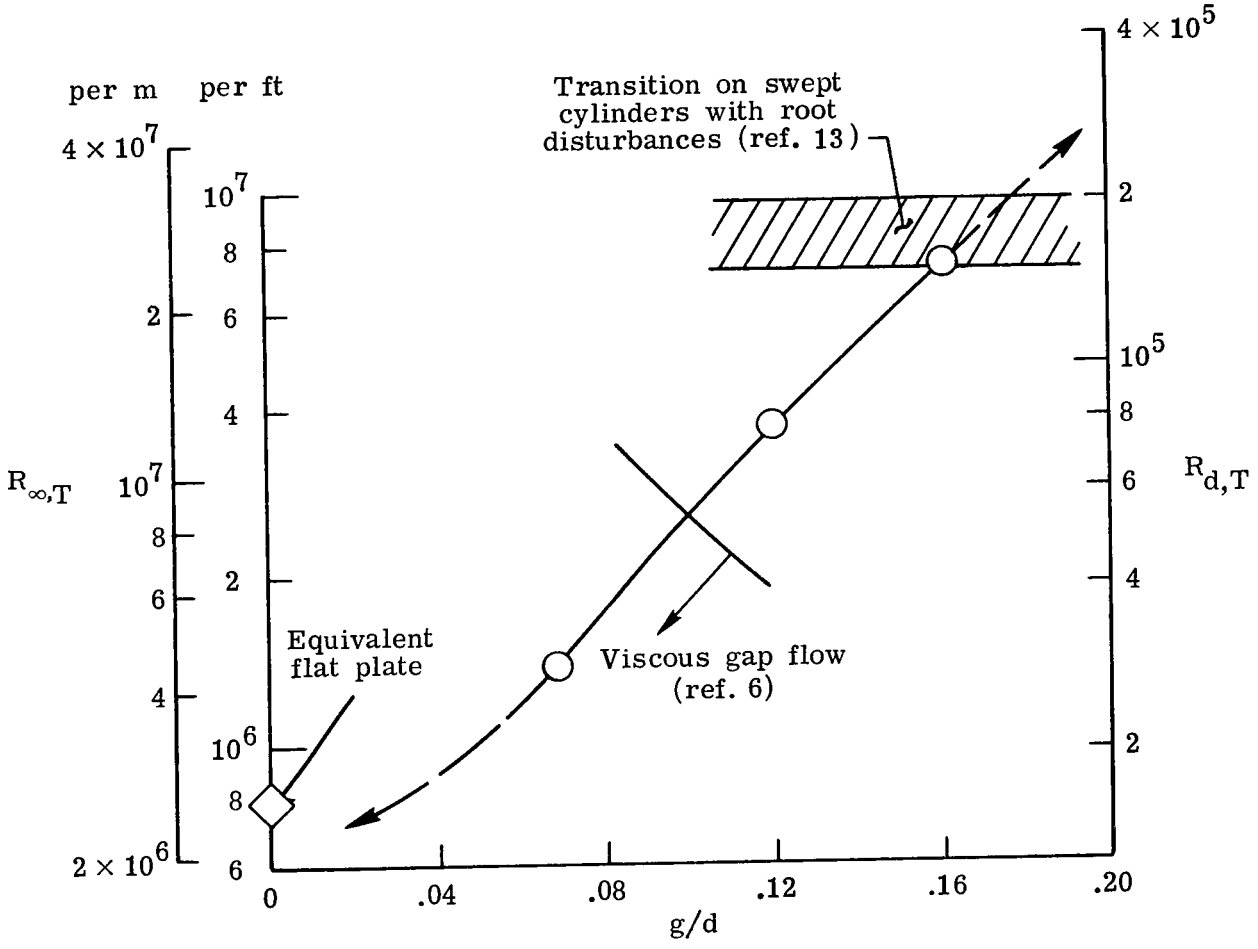

Figure 15.- Effect of gap width on transition Reynolds number at model base. $\alpha = 10^{o}$; d = 0.635 cm (0.25 in.).

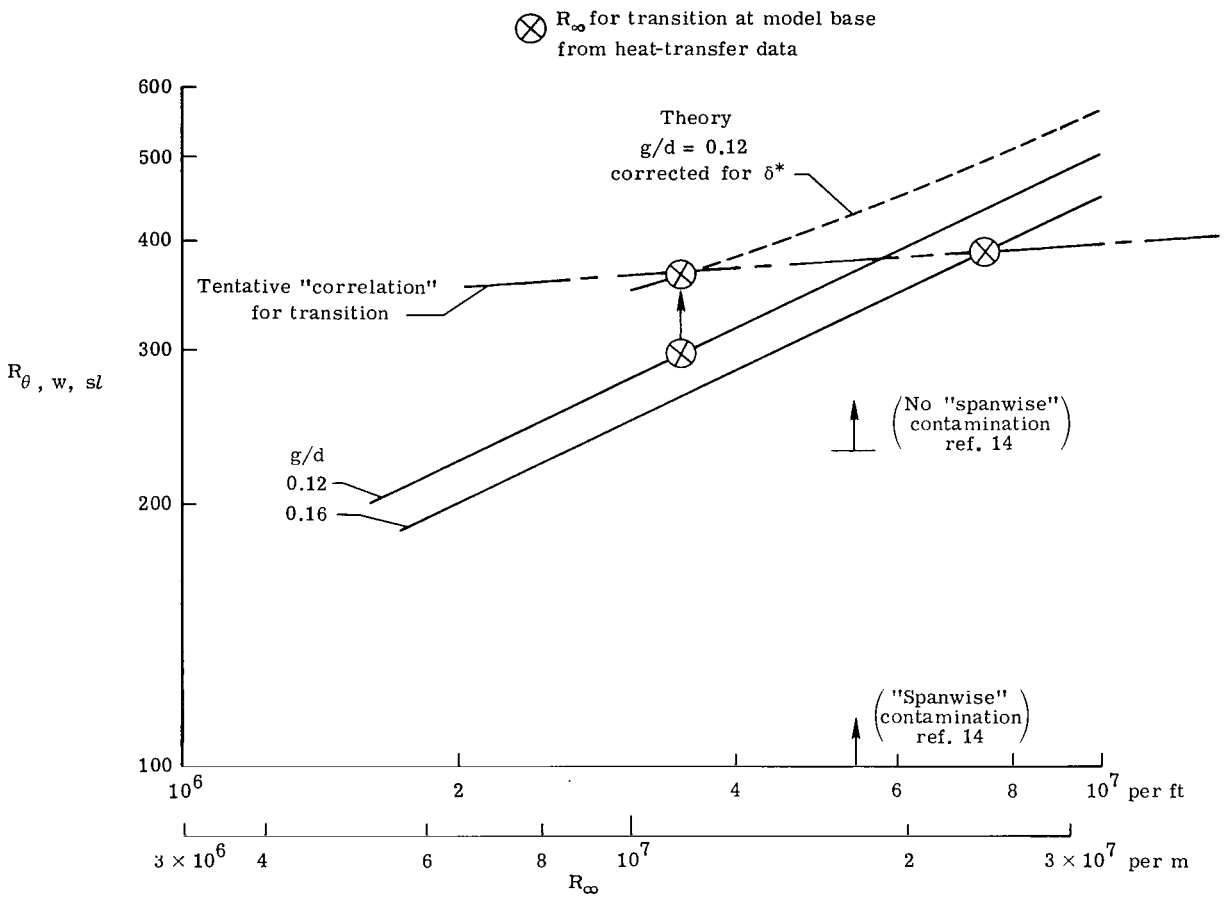

(a) Theoretical variations of $R_{\theta,w,sl}$ with R_∞.

Figure 16.- Stagnation-line momentum thickness Reynolds number as a criterion for transition.

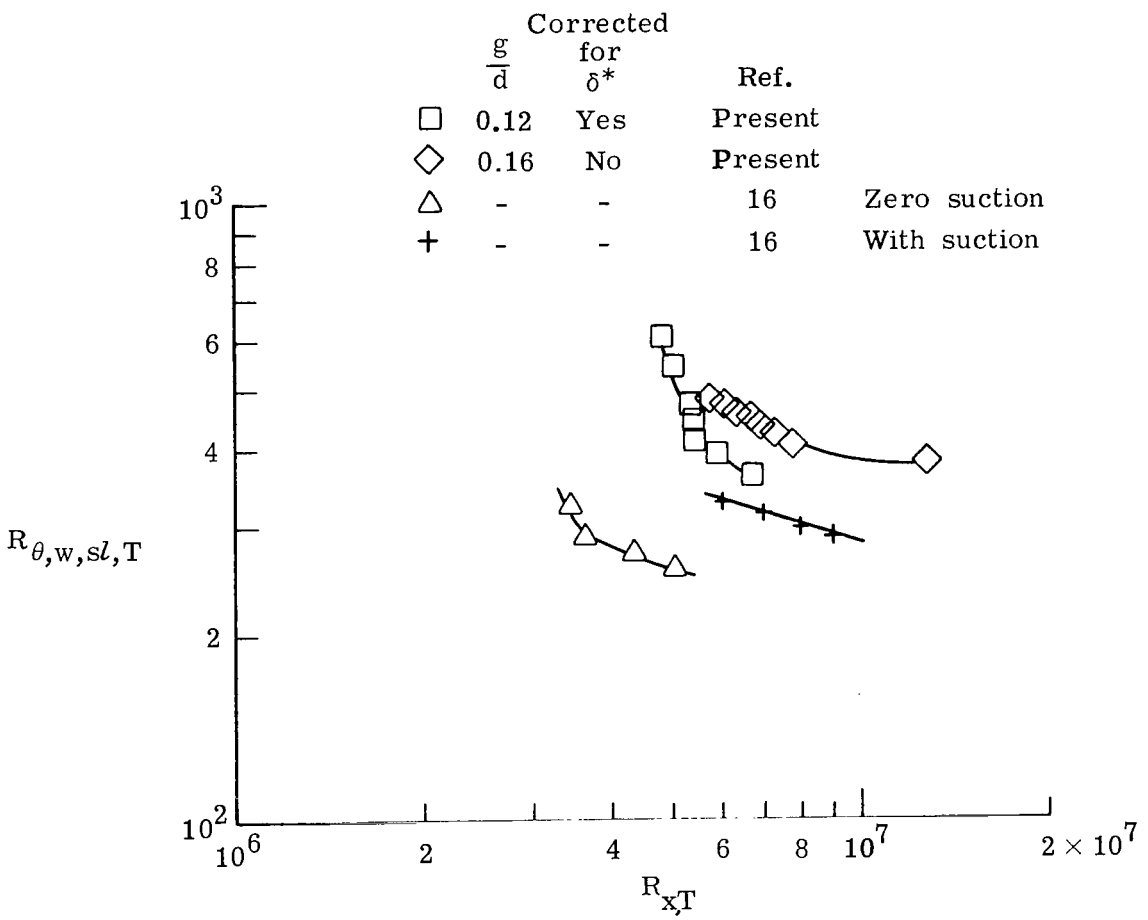

(b) Variation of momentum thickness Reynolds number at transition with transition Reynolds number based on x_T.

Figure 16.- Concluded.

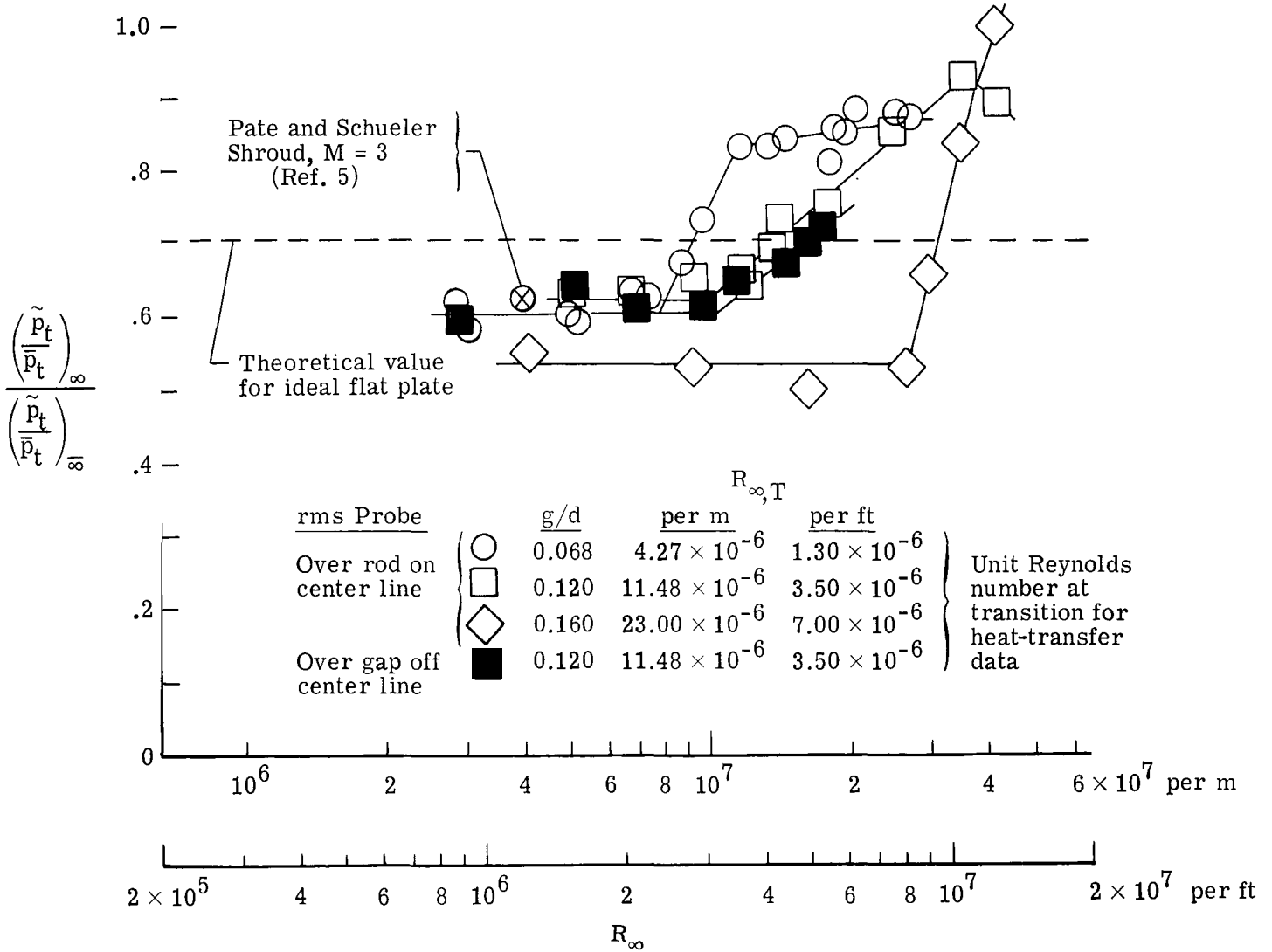

Figure 17.- Variation with R_∞ of normalized root-mean-square pitot pressure with unit Reynolds number.

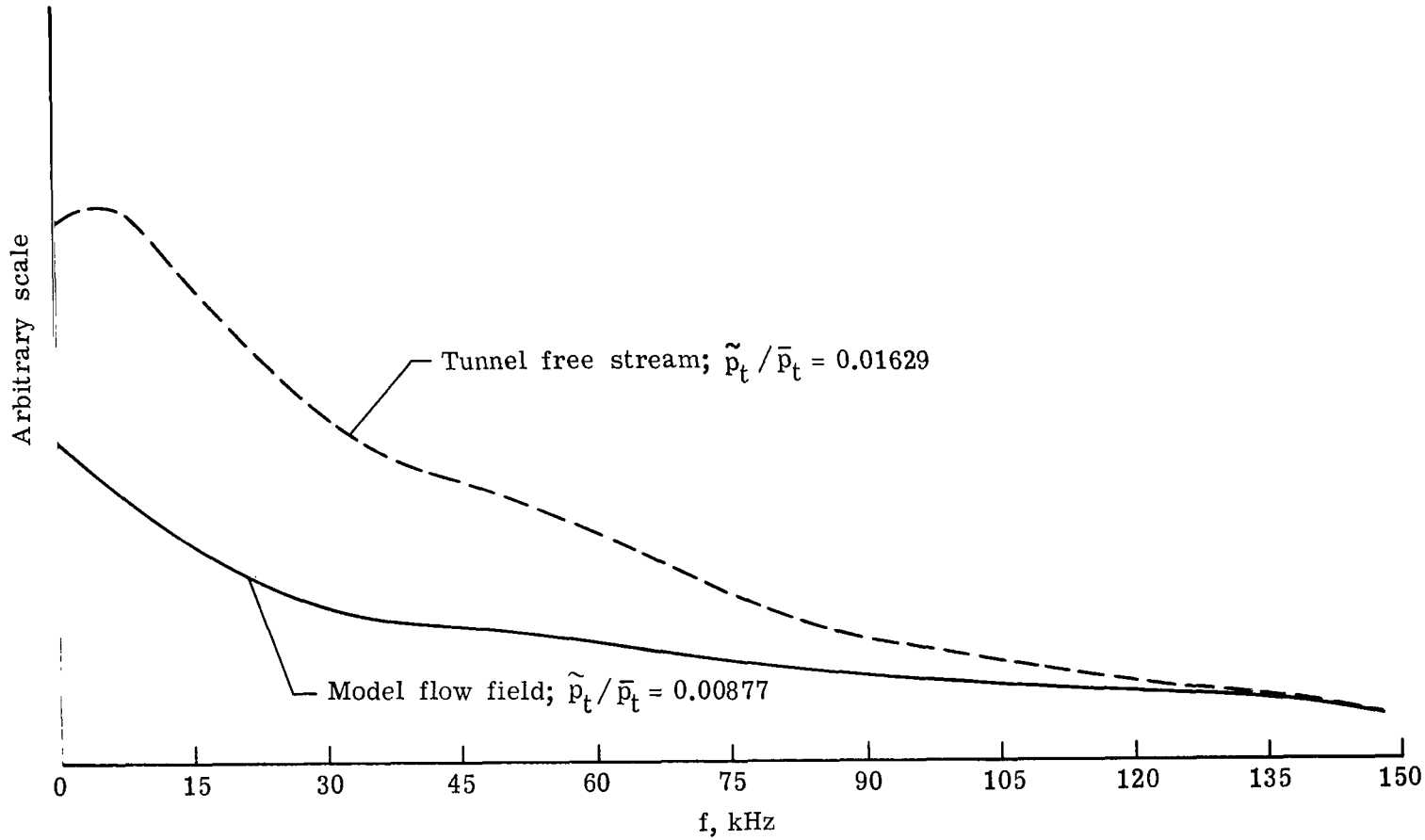

(a) Laminar; $R_{\infty} = 17.8 \times 10^6$ per m (5.42×10^6 per ft); $R_{\infty} = 26.3 \times 10^6$ per m (8×10^6 per ft).

Figure 18.- Spectra of pressure fluctuations in tunnel free stream and in model flow field (ref. 6). $M_{\infty} = 6$; $\alpha = 10^{\circ}$; g/d = 0.16.

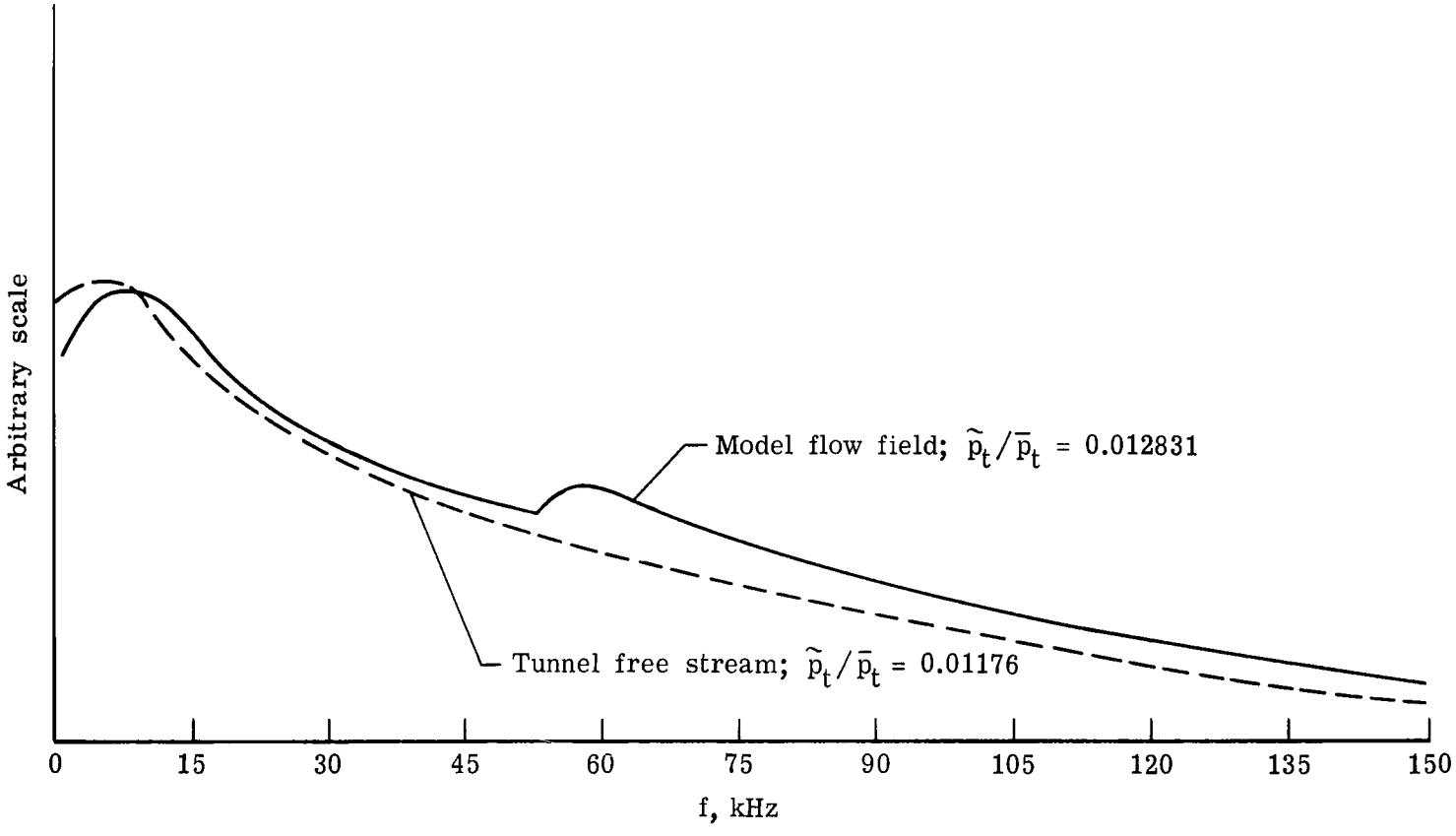

(b) Turbulent; $R_{\overline{\infty}} = 28.7 \times 10^6$ per m (8.73×10^6 per ft); $R_\infty = 42.7 \times 10^6$ per m (13×10^6 per ft).

Figure 18.- Concluded.

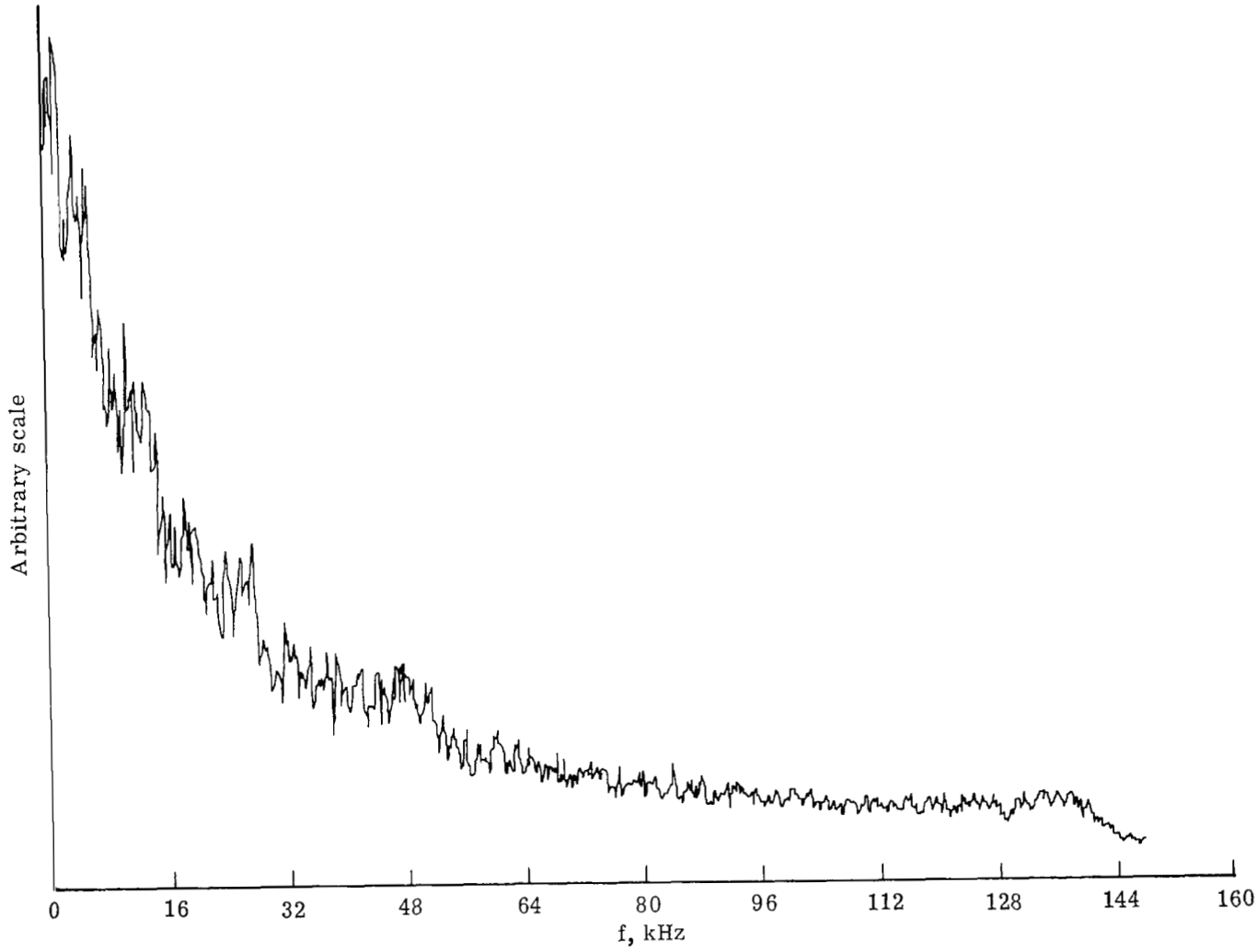

(a) $g/d = 0.068$; $R_{\infty} = 4.98 \times 10^6$ per m $(1.52 \times 10^6$ per ft); $\tilde{p}_t/\bar{p}_t = 0.013$.

Figure 19.- Typical spectra in flow field of rod model when boundary layer on rods is laminar. $M_{\infty} = 6$; $\alpha = 10^{\circ}$.

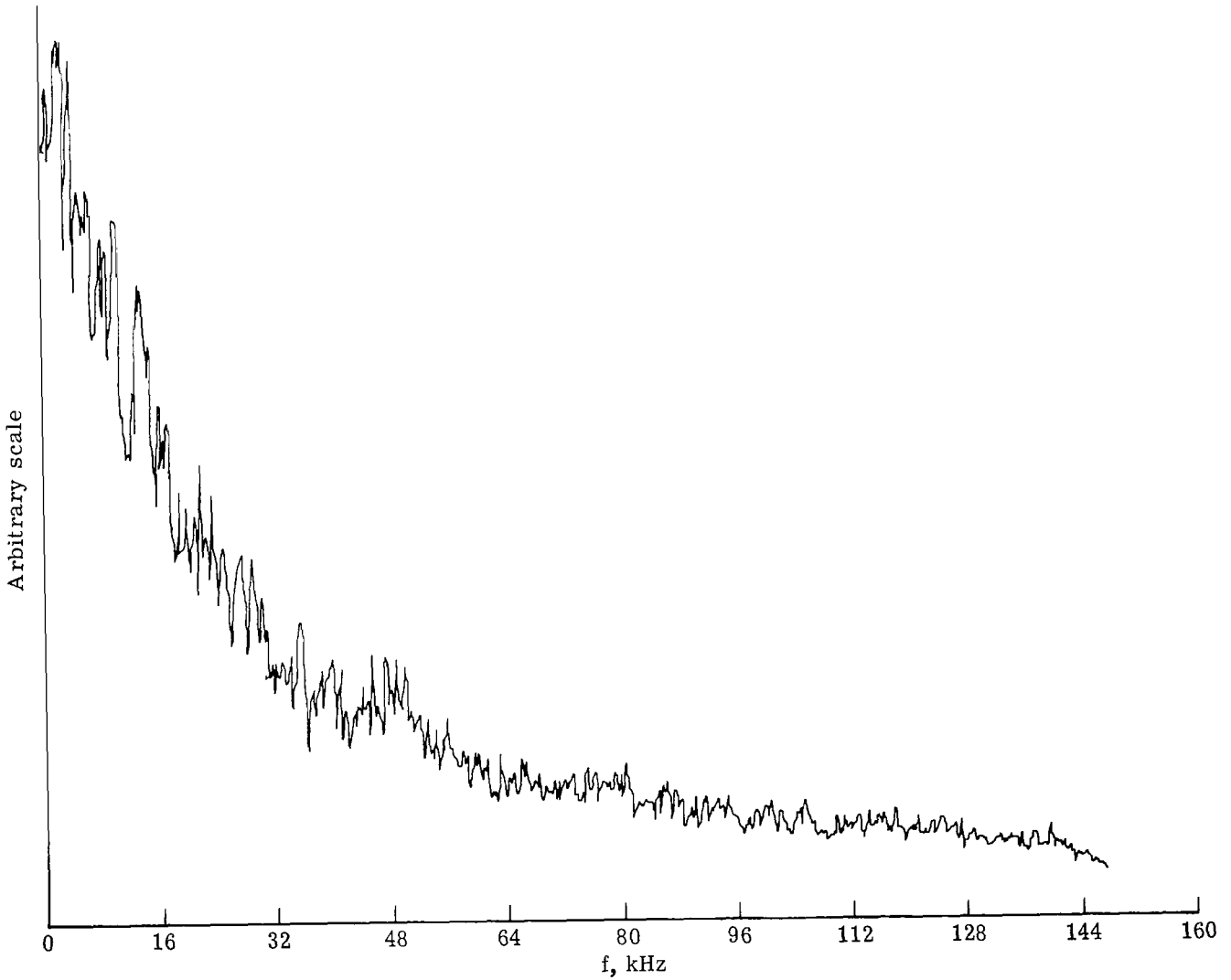

(b) g/d = 0.120; probe over gap; $R_{\overline{\infty}} = 5.18 \times 10^6$ per m (1.58×10^6 per ft); $\tilde{p}_t/\bar{p}_t = 0.014$.

Figure 19.- Continued.

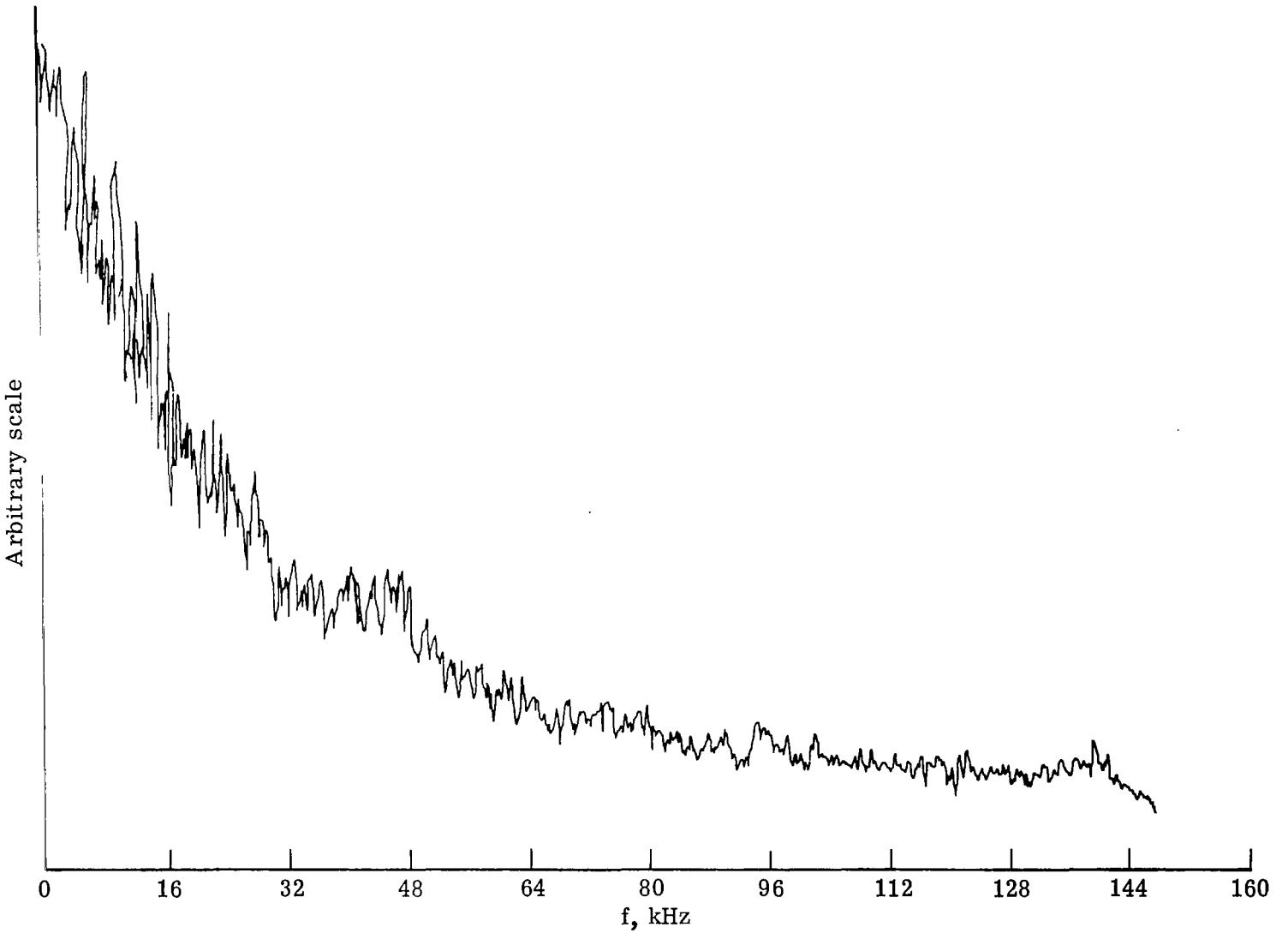

(c) g/d = 0.120; probe over rod; $R_{\infty} = 5.04 \times 10^6$ per m (1.54×10^6 per ft); $\tilde{p}_t/\tilde{p}_t = 0.013$.

Figure 19.- Continued.

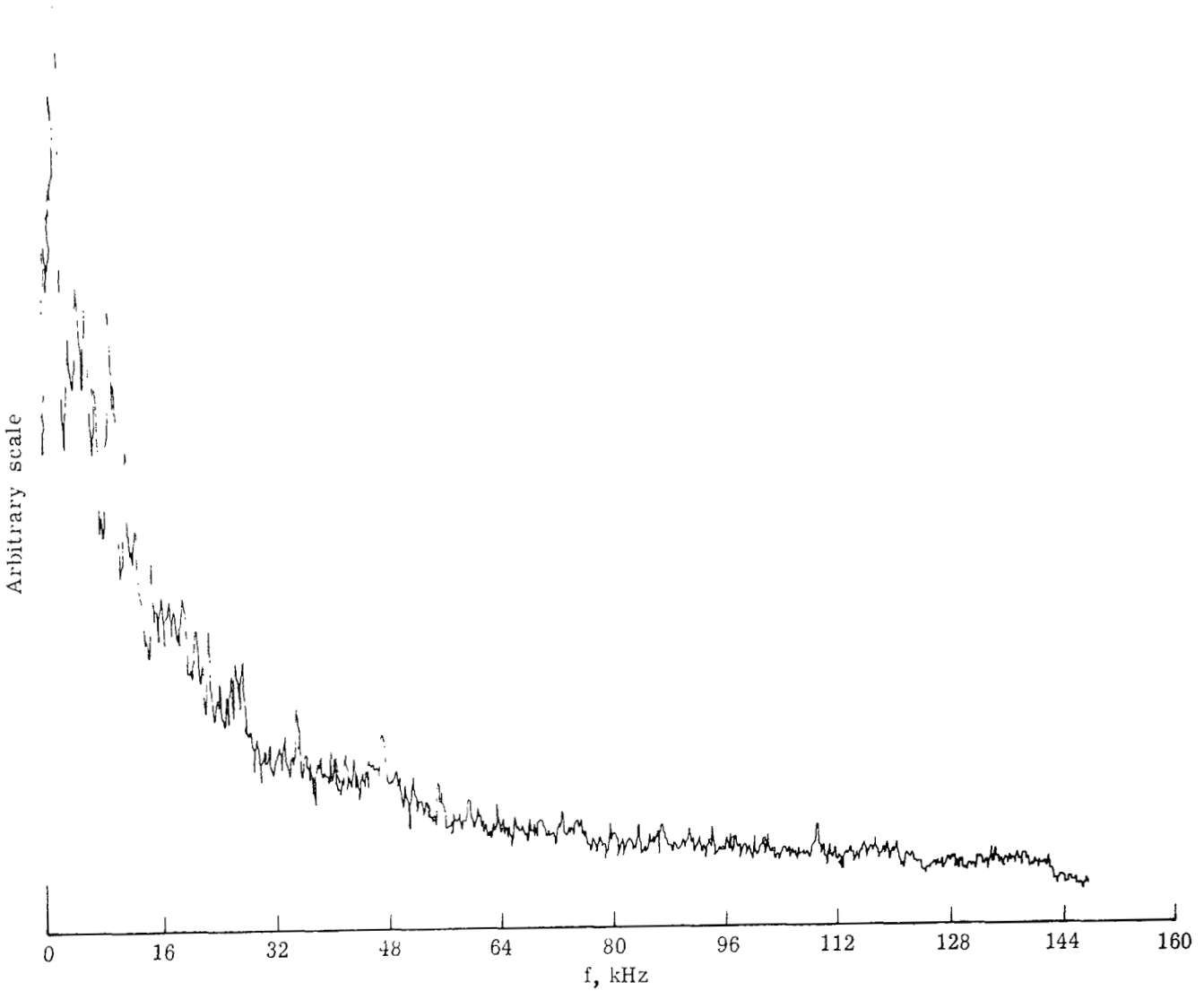

(d) Free stream; $R_{\infty} = 3.28 \times 10^6$ per m (0.987×10^6 per ft); $\tilde{p}_t/\bar{p}_t = 0.022$.

Figure 19.- Concluded.

NATIONAL AERONAUTICS AND SPACE ADMINISTRATION
WASHINGTON, D.C. 20546

OFFICIAL BUSINESS
PENALTY FOR PRIVATE USE $300

SPECIAL FOURTH-CLASS RATE BOOK

POSTAGE AND FEES PAID
NATIONAL AERONAUTICS AND SPACE ADMINISTRATION
451

U.S.MAIL

985 001 C1 U A 751010 S00903DS
DEPT OF THE AIR FORCE
AF WEAPONS LABORATORY
ATTN: TECHNICAL LIBRARY (SUL)
KIRTLAND AFB NM 87117

POSTMASTER: If Undeliverable (Section 158 Postal Manual) Do Not Return

"The aeronautical and space activities of the United States shall be conducted so as to contribute . . . to the expansion of human knowledge of phenomena in the atmosphere and space. The Administration shall provide for the widest practicable and appropriate dissemination of information concerning its activities and the results thereof."

—NATIONAL AERONAUTICS AND SPACE ACT OF 1958

NASA SCIENTIFIC AND TECHNICAL PUBLICATIONS

TECHNICAL REPORTS: Scientific and technical information considered important, complete, and a lasting contribution to existing knowledge.

TECHNICAL NOTES: Information less broad in scope but nevertheless of importance as a contribution to existing knowledge.

TECHNICAL MEMORANDUMS: Information receiving limited distribution because of preliminary data, security classification, or other reasons. Also includes conference proceedings with either limited or unlimited distribution.

CONTRACTOR REPORTS: Scientific and technical information generated under a NASA contract or grant and considered an important contribution to existing knowledge.

TECHNICAL TRANSLATIONS: Information published in a foreign language considered to merit NASA distribution in English.

SPECIAL PUBLICATIONS: Information derived from or of value to NASA activities. Publications include final reports of major projects, monographs, data compilations, handbooks, sourcebooks, and special bibliographies.

TECHNOLOGY UTILIZATION PUBLICATIONS: Information on technology used by NASA that may be of particular interest in commercial and other non-aerospace applications. Publications include Tech Briefs, Technology Utilization Reports and Technology Surveys.

Details on the availability of these publications may be obtained from:

SCIENTIFIC AND TECHNICAL INFORMATION OFFICE

NATIONAL AERONAUTICS AND SPACE ADMINISTRATION

Washington, D.C. 20546